doi.org/10.26434/chemrxiv.11288675.v1

Nickel(II)-Methyl Complexes Adopting Idealized Seesaw Geometries

Ethan A. Hill, Norman Zhao, Alexander S. Filatov, John Anderson

Submitted date: 27/11/2019 • Posted date: 06/12/2019

Citation information: Hill, Ethan A.; Zhao, Norman; Filatov, Alexander S.; Anderson, John (2019): Nickel(II)-Methyl Complexes Adopting Idealized Seesaw Geometries. ChemRxiv. Preprint. https://doi.org/10.26434/chemrxiv.11288675.v1

We report four-coordinate nickel(II)-methyl complexes of tris-carbene borate ligands which adopt rare seesaw geometries. Experimental and computational results suggest the structural distortion from threefold symmetry results from a combination of electronic stabilization of the singlet state, strong field donors, and constrained angles from the chelating ligand.

File list (3)

COMMUNICATION

Nickel(II)-Methyl Complexes Adopting Idealized Seesaw Geometries

Received 00th January 20xx,
Accepted 00th January 20xx

DOI: 10.1039/x0xx00000x

Ethan A. Hill†, Norman Zhao†, Alexander S. Filatov, John S. Anderson*

We report four-coordinate nickel(II)-methyl complexes of tris-carbene borate ligands which adopt rare seesaw geometries. Experimental and computational results suggest the structural distortion from threefold symmetry results from a combination of electronic stabilization of the singlet state, strong field donors, and constrained angles from the chelating ligand.

Nickel-alkyl complexes have been invoked as important intermediates in a host of chemical transformations including the production of acetic acid and cross-coupling reactions.[1–6] In all reported examples of crystallographically characterized Ni(II)-methyl complexes, a diamagnetic, square planar geometry is observed.[7,8] Despite this, catalytically active Ni(II)-alkyl species may likely exhibit or transition through different coordination geometries.[9–11] For example, other synthetic Ni(II) complexes can be found in tetrahedral geometries in addition to the more common square planar geometries. While a square planar geometry is favored due to electronic stabilization of the d^8 nickel(II) ion, a tetrahedral geometry may be favoured with suitably bulky or chelating ligands.[12]

An alternative geometry for four-coordinate metal centers that has rarely been observed is a seesaw geometry. In fact, only a handful of examples of nickel(II) complexes in this geometry have been reported.[10,13–15] In these cases, steric bulk is used to enforce the desired geometry. For example, the first of these reported by Bröring and co-workers utilized a tripyrranato ligand which positions methyl substituents within the square plane, forcing halide ligands above this plane.[16–18] Other examples include those by Gossage and Baruah where homoleptic complexes of Ni(II) were synthesized with bulky propan-2-ylidene and oxazoline substituents that prevent planarization of the Ni(II) coordination environment.[11,19] Another recent example of a seesaw geometry at a Ni(II) center involves a diisopropylpyrazole-substituted carbazole ligand to enforce steric crowding of the square plane.[10] Finally, an example of a ligand-constrained geometry around a Ni(II) center can be seen in a complex bound to a triphosphacyclododecane ligand.[20] This ligand binds in a facial manner with strongly donating trialkylphosphines which are proposed to enforce a low-spin state at nickel. Due to the constrained ligand environment, the coordination geometry distorts to accommodate the low-spin state but cannot fully isomerize to a square planar geometry. These examples demonstrate the lengths required to enforce this unusual geometry at a d^8 Ni(II) center.

We have been interested in exploring the chemistry of late transition metals supported by chelating and strongly donating tris-carbene borate scaffolds.[21,22] These ligand scaffolds typically enforce a pseudo-tetrahedral geometry, but also favor low-spin states due to the strong donor properties of the carbene ligands. These factors suggest that Ni(II) complexes supported by this ligand would have geometric frustration between an electronically preferred square planar geometry and a chelate-enforced pseudo-tetrahedral geometry. We therefore rationalized that Ni(II) complexes of this ligand with suitably strong ligand fields might display unusual geometries and electronic structures.[23–25] Here we report the isolation and characterization of two Ni(II)-methyl complexes supported by a

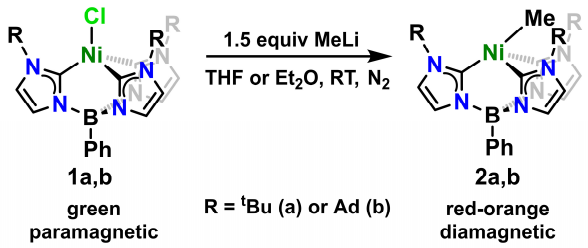

Scheme 1. Synthesis of complexes **2a** and **2b**.

† These authors contributed equally

* *Dr. E. A. Hill, N. Zhao, Dr. A. S. Filatov, and Prof. J. S. Anderson*
Department of Chemistry
The University of Chicago
5735 S. Ellis Ave
Chicago, IL 60637 (USA)
E-mail: jsanderson@uchicago.edu

Electronic SI (ESI) available: [details of any SI available should be included here]. See DOI: 10.1039/x0xx00000x

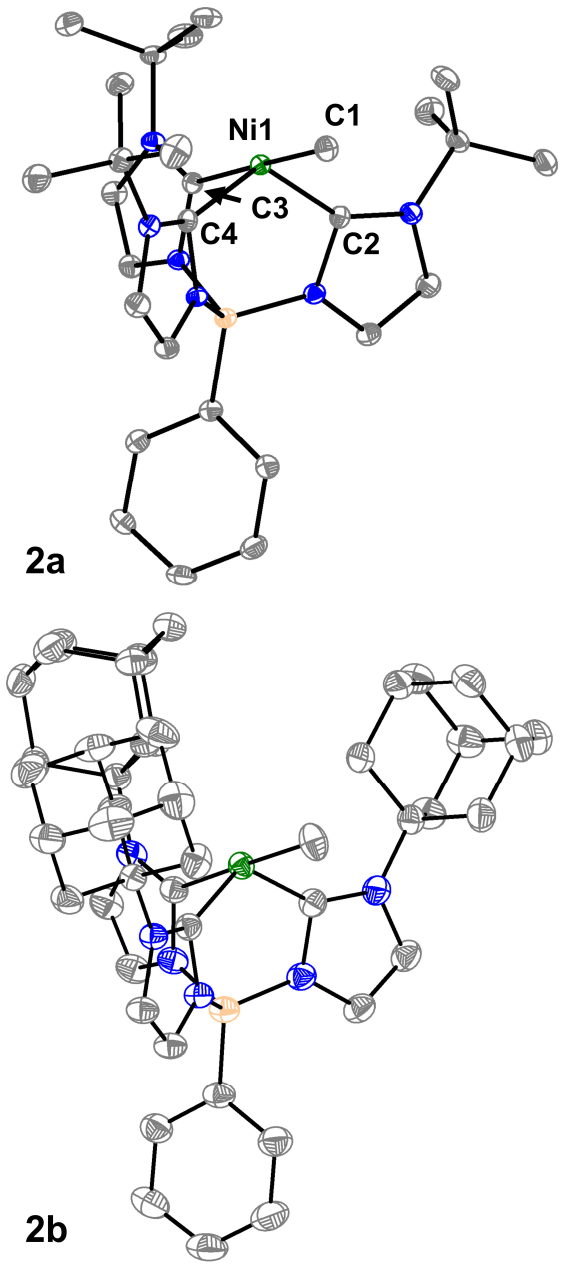

Figure 1. SXRD structures of **2a** and **2b**. Ellipsoids are shown at 50% and H atoms are omitted for clarity. Ni is shown in green, N in blue, B in tan, and C in gray. Atom labels for **2b** are the same as those depicted for **2a**. Selected bond lengths (Å) and angles (°) and geometric parameters for **2a**: Ni1–C1 = 1.965(2), Ni1–C2 = 1.895(2), Ni1–C3 = 1.922(2), Ni1–C4 = 1.887(2), C1–Ni1–C3 = 177.19(8), C2–Ni1–C4 = 121.49(8), τ_4 = 0.43. For **2b**: Ni1–C1 = 1.959(2), Ni1–C2 = 1.886(2), Ni1–C3 = 1.912(2), Ni1–C4 = 1.884(2), C1–Ni1–C3 = 177.79(7), C2–Ni1–C4 = 121.25(7), τ_4 = 0.43.

strongly donating tris-carbene borate ligand which occupy idealized seesaw geometries.

The Ni(II)-chloride complexes were first synthesized by initial deprotonation of the proligand, $[PhB(RImH)_3][OTf]_2$ (where R = ^{t}Bu or Ad), with *in situ* generated lithium diisopropylamide (LDA) followed by metalation with tetraethylammonium tetrachloronickelate ($[Et_4N]_2[NiCl_4]$) to yield $PhB(^t BuIm)_3NiCl$ and $PhB(AdIm)_3NiCl$ (**1a** and **1b**) in low but synthetically viable yields (see SI). The title complexes, $PhB(^t BuIm)_3NiMe$ and $PhB(AdIm)_3NiMe$ (**2a** and **2b**), were synthesized by treatment of the Ni(II)-chloride complexes **1a** and **1b** with a solution of methyllithium following a similar reported procedure for related complexes of cobalt (Scheme 1).[26] Complexes **2a** and **2b** can be isolated as red, microcrystalline solids in good yield. These complexes are thermally unstable at room temperature, but pure solids can be stored at −35 °C for weeks to months without noticeable decomposition. Despite their intense, red-orange color in solution, complexes **2a** and **2b** display no distinct absorption features by UV-vis spectroscopy with only trailing absorbances from the UV region of the spectra into the visible region. Contrary to the parent Ni(II)-chloride complexes **1a** and **1b**, both complexes **2a** and **2b** are diamagnetic. However, ^{1}H NMR spectra of both the Cl and Me complexes in C_6D_6 indicate C_3-symmetric geometries in solution at room temperature (see SI).

We then turned to single-crystal X-ray diffraction (SXRD) measurements to probe the structures of these Ni complexes in the solid-state. As expected from their threefold symmetric NMR spectra, complexes **1a** and **1b** are pseudo-tetrahedral in the solid-state and have a C_3 axis with a B-Ni-Cl angle of 177.92(6)° and 178.8(2)°, respectively (see SI). In contrast, while the room temperature ^{1}H NMR spectra of the methyl complexes **2a** and **2b** are consistent with a C_3-symmetric structure, an unusual seesaw coordination geometry at the Ni(II) centers is observed in their solid-state structures (Figure 1). The metrical parameters of the Ni centers in complexes **2a** and **2b** are consistent with a nearly perfect seesaw geometry around the Ni(II) center composed of three carbon donors from the tris-carbene borate ligand and a fourth from the bound methyl group. The Ni-methyl carbon atom distances are nearly identical between the two complexes at 1.965(2) and 1.959(2) Å, respectively. The two widest C-Ni-C angles which describe the seesaw geometry are 177.19(8)° and 121.49(8)° for **2a** and 177.80(7)° and 121.25(7)° for **2b**. Using both of these angles, a geometry index parameter τ_4 can be calculated to describe the coordination environment of the Ni(II) center between square planar (τ_4 = 0), tetrahedral (τ_4 = 1), or seesaw (τ_4 = 0.43).[27,28] For both **2a** and **2b**, the τ_4 parameter is calculated to be 0.43, indicating an idealized seesaw geometry around the Ni(II) center. These are the first such cases to be crystallographically characterized.[§]

With the disparity between solid-state and solution structural data, we sought to better understand the dynamics of complexes **2a** and **2b** in solution. Variable temperature ^{1}H NMR experiments were conducted in d_8-toluene to determine an isomerization barrier, $\Delta G^{\ddagger}$ (Figure 2).[29,30] In these complexes, the barrier being measured represents the energy to reorient the methyl substituent from between one pair of imidazole groups to between a different pair through either an effective lever mechanism or via B-Ni-Me linearization to a C_3-symmetric isomer (see below).[31] For an imidazole resonance of **2a** (labeled with an asterisk in Figure 2), a coalescence temperature of 215 K was determined and from the value of $\Delta\nu$, the peak-to-peak splitting in Hz of the fully resolved asymmetric structure, a

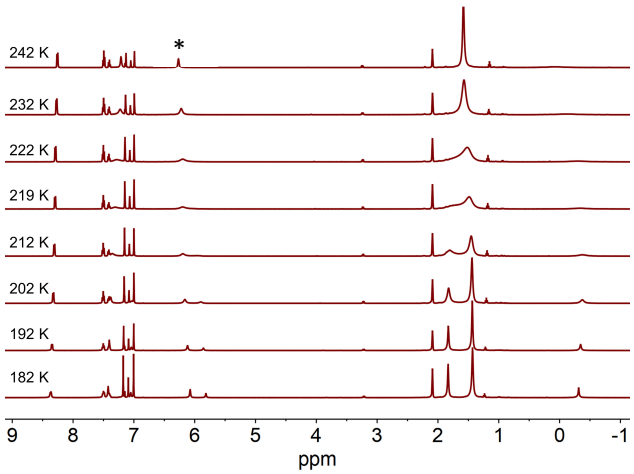

Figure 2. Variable temperature ^{1}H NMR spectra for complex **2a** in d_8-toluene showing the splitting of the peaks of the imidazole groups as temperature decreases. These data were used to determine coalescence temperature and calculate $\Delta G^{\ddagger}$ for the isomerization process. Asterisk marks resonance used for in-text values.

barrier to isomerization was calculated to be 10.4±0.5 kcal/mol. In the case of **2b** with the larger adamantyl groups, we anticipated a higher calculated barrier. However, the calculated value for the analogous imidazole proton resonance is the same within an estimate of the error. From the coalescence temperature of 225 K and the measured $\Delta\nu$ values, a barrier of 10.9±0.5 kcal/mol was calculated (see SI). This suggests that while the adamantyl groups are bulkier, extending further away from the Ni center, this does not appreciably alter the barrier to isomerization in this complex.

A point of interest upon studying complexes **2a** and **2b** was to rationalize the observed seesaw structures in the solid-state. A crude examination of the geometries a 4-coordinate Ni(II) complex may adopt indicates three possible isomers as discussed above: tetrahedral, square planar, and seesaw. The parent chloride complexes **1a** and **1b** are characterized as high-spin S = 1 complexes in a pseudo-tetrahedral geometry. Given the additional strong field methyl ligand in complexes **2a** and **2b**, it is likely that diamagnetic, low-spin Ni(II) species would be most stable.[32] Because of this, pseudo-tetrahedral geometries are now disfavored, as this coordination environment would result in occupation of a high energy, antibonding orbital and Jahn-Teller distortion of a nominally degenerate set of orbitals. To remove this energetic penalty, most low-spin Ni(II) complexes are found in square planar geometries. This splits the degeneracy of the high energy orbital pair to stabilize one fully filled orbital while leaving a higher energy empty orbital, typically d_{x2-y2}. It is proposed in the case of complexes **2a** and **2b** that the chelate ring of the tris-carbene borate ligand prevents distortion to a square planar geometry that would be otherwise electronically favored. As a result, the intermediate seesaw geometry is most stable, distorted away from pseudo-tetrahedral but restricted from planarization.

This qualitative description of the preference for seesaw geometries observed in complexes **2a** and **2b** is also supported by density functional theory (DFT) calculations. The geometry optimization of **2a** in a singlet electronic configuration yields a structure that is in agreement with its solid-state structure. Geometry optimization of **2a** in a triplet state shows instead a pseudo-tetrahedral geometry, similar to the geometry seen in **1a** and **1b** (see SI). The DFT calculations predict the S = 0 seesaw geometry to be 31 kcal/mol lower in energy than the corresponding S = 0 pseudo-tetrahedral isomer but only 11 kcal/mol lower than the S = 1 threefold symmetric species (see SI). Comparison of the frontier molecular orbitals of **2a** reveals that deviation from a pseudo-tetrahedral to seesaw geometry stabilizes the d_{z^2} orbital (Figure 3). This results in a single, high-lying d_{x2-y2} orbital that remains unoccupied with a clustering of occupied orbitals at overall lower energy than those in the pseudo-tetrahedral geometry. Additionally, it is worth noting that the d_{z^2} orbital in the pseudo-tetrahedral geometry is significantly raised in energy compared to a classical depiction of the d-orbital splitting pattern for this geometry and likely arises due to the strong donating ability of the methyl ligand. Finally, the qualitative orbital depiction for the seesaw geometry is similar to the classical depiction of square planar d-orbital splitting, further suggesting such a geometry would be preferred in this system if not for the chelate ring constraint imposed by the tris-carbene borate ligand.

The DFT calculations above suggest that an isomerization mechanism involving a linear S = 1 transition state is energetically reasonable, but we also wanted to probe the feasibility of a lever type mechanism for this isomerization computationally. The C_{Me}-Ni-$C_{carbene}$-$N_{carbene}$ dihedral angle was held fixed at 0° and the Ni-Me group allowed to move between a pseudo-tetrahedral orientation and close proximity to the R-group of the imidazole in order to find a low energy intermediate which would model the transition state for this isomerization (see SI). In doing so, a conformer higher in energy by 20 kcal/mol relative to the seesaw geometry was found. This energy is high enough to rule out this pathway as operative given the ~10 kcal/mol energy barrier calculated from the variable temperature experiments. Given the computed

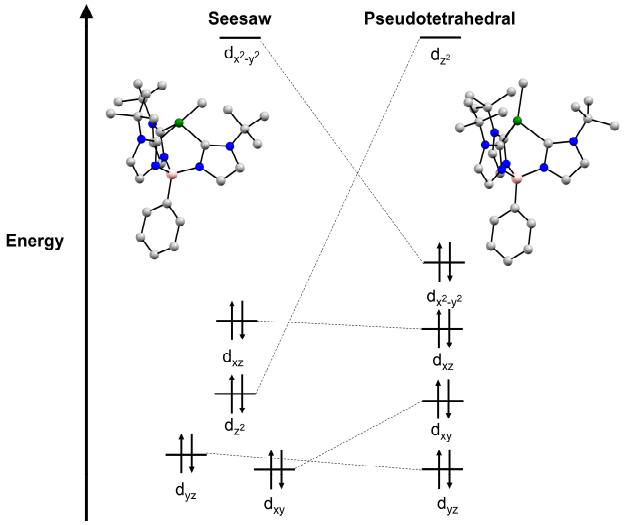

Figure 3. Qualitative Walsh diagram depicting the relative energies of the d-orbitals for the seesaw and pseudo-tetrahedral geometries determined from DFT calculations of the geometry optimized singlet of **2a**. Basis set/functional used: def2-TZVPP on Ni, N, and C bound to Ni, def2-SVP on all other atoms/O3LYP.

relative energies of the S = 0 (+31 kcal/mol) and S = 1 (+11 kcal/mol) pseudo-tetrahedral isomers, it is likely that the isomerization proceeds through the S = 1 C_3-symmetric isomer. This conclusion is also supported by the relatively broad Ni-CH_3 proton resonance at room temperature that displays a large change in chemical shift upon cooling. This effect is likely the result of perturbation from a minor amount of the paramagnetic, pseudo-tetrahedral isomer at room temperature as has been previously observed.[33] Interestingly, this observation suggests that paramagnetic Ni-methyl intermediates are accessible at room temperature in the current system, and that similarly high-spin Ni(II)-alkyl complexes may be reasonable intermediates in catalysis.

The Ni(II)-methyl complexes **2a** and **2b** are the first examples of such species to be found in a seesaw coordination geometry as revealed by their solid-state structures. Variable temperature ^{1}H NMR spectroscopy demonstrates that this distortion also occurs in the solution state and has an electronic origin as opposed to arising from any solid-state crystal packing. Using density functional theory calculations, the observed structures are rationalized by an overall lowering of filled orbitals by distortion from pseudo-tetrahedral to a seesaw geometry. This geometry is proposed to be favored over square planar geometry due to the constraint of the tris-carbene borate ligand. This work shows that Ni-alkyl species with chelating ligands can adopt this geometry and draws attention to the potential effects of this distortion and electronic structure on the reactivity of Ni intermediates in catalytic transformations.

Conflicts of interest

There are no conflicts to declare.

Notes and references

This work was supported by the NSF through a CAREER award to JSA, CHE-1654144 and a GRFP award to NZ DGE-1746045. NSF's ChemMatCARS Sector 15 is principally supported by the Divisions of Chemistry (CHE) and Materials Research (DMR), National Science Foundation, under grant number NSF/CHE-1834750. Use of the Advanced Photon Source, an Office of Science User Facility operated for the U.S. Department of Energy (DOE) Office of Science by Argonne National Laboratory, was supported by the U.S. DOE under Contract No. DE-AC02-06CH11357.

§ Determined by searching the Cambridge Crystallographic Database using Conquest by limiting a 4-coordinate Ni center with two pairs of ligand bond angles restricted between 150-180° and 110-130°.

1 P. A. Lindahl, *J. Biol. Inorg. Chem.*, 2004, **9**, 516–524.
2 X. Zhao, H.-Y. Tu, L. Guo, S. Zhu, F.-L. Qing and L. Chu, *Nat. Commun.*, 2018, **9**, 3488.
3 L. Guo and M. Rueping, *Acc. Chem. Res.*, 2018, **51**, 1185–1195.
4 J. Hu, Y. Zhao, J. Liu, Y. Zhang and Z. Shi, *Angew. Chem., Int. Ed.*, 2016, **55**, 8718–8722.
5 D. Nianios, S. Thierbach, L. Steimer, P. Lulchev, D. Klostermeier and S. Fetzner, *BMC Biochem.*, 2015, **16**, 10.
6 M. Can, F. A. Armstrong and S. W. Ragsdale, *Chem. Rev.*, 2014, **114**, 4149–4174.
7 E. Carmona, F. González, M. L. Poveda, J. L. Atwood and R. D. Rogers, *J. Chem. Soc., Dalt. Trans.*, 1980, 2108–2116.
8 P. Stoppioni, P. Dapporto and L. Sacconi, *Inorg. Chem.*, 1978, **17**, 718–725.
9 S. A. Macgregor, Z. Lu, O. Eisenstein and R. H. Crabtree, *Inorg. Chem.*, 1994, **33**, 3616–3618.
10 J. Ghannam, T. Al Assil, T. C. Pankratz, R. L. Lord, M. Zeller and W.-T. Lee, *Inorg. Chem.*, 2018, **57**, 8307–8316.
11 A. Tarai and J. B. Baruah, *Dalton Trans.*, 2018, **47**, 4921–4930.
12 T. A. Albright, J. K. Burdett and M.-H. Whangbo, *Orbital Interactions in Chemistry*, John Wiley & Sons, Inc., Hoboken, NJ, USA, 2nd edn., 2013.
13 C. A. Grapperhaus, J. A. Bellefeuille, J. H. Reibenspies and M. Y. Darensbourg, *Inorg. Chem.*, 1999, **38**, 3698–3703.
14 R. Graziani, M. Vidali, U. Casellato and P. A. Vigato, *Transit. Met. Chem.*, 1978, **3**, 99–103.
15 J. Li, D. Tian, H. Song, C. Wang, X. Zhu, C. Cui and J. P. Cheng, *Organometallics*, 2008, **27**, 1605–1611.
16 M. Bröring, S. Prikhodovski and C. D. Brandt, *J. Chem. Soc., Dalt. Trans.*, 2002, 4213–4218.
17 M. Bröring, S. Prikhodovski and C. D. Brandt, *Inorganica Chim. Acta*, 2004, **357**, 1733–1738.
18 M. Bröring, S. Prikhodovski, C. D. Brandt and E. C. Tejero, *Chem. Eur. J.*, 2007, **13**, 396–406.
19 J. A. Adjei, A. J. Lough and R. A. Gossage, *RSC Adv.*, 2019, **9**, 3956–3964.
20 P. G. Edwards, F. Ingold and M. B. Hursthouse, *Chem. Commun.*, 1998, 545–546.
21 M. K. Goetz, E. A. Hill, A. S. Filatov and J. S. Anderson, *J. Am. Chem. Soc.*, 2018, **140**, 13176–13180.
22 M. K. Goetz and J. S. Anderson, *J. Am. Chem. Soc.*, 2019, **141**, 4051–4062.
23 R. A. Juarez, W.-T. Lee, J. M. Smith and H. Wang, *Dalton Trans.*, 2014, **43**, 14689–14695.
24 I. Nieto, R. P. Bontchev and J. M. Smith, *Eur. J. Inorg. Chem.*, 2008, **2008**, 2476–2480.
25 S. B. Muñoz, W. K. Foster, H.-J. Lin, C. G. Margarit, D. A. Dickie and J. M. Smith, *Inorg. Chem.*, 2012, **51**, 12660–12668.
26 R. E. Cowley, R. P. Bontchev, E. N. Duesler and J. M. Smith, *Inorg. Chem.*, 2006, **45**, 9771–9779.
27 L. Yang, D. R. Powell and R. P. Houser, *Dalton Trans.*, 2007, 955–964.
28 D. Rosiak, A. Okuniewski and J. Chojnacki, *Polyhedron*, 2018, **146**, 35–41.
29 H. Shanan-Atidi and K. H. Bar-Eli, *J. Phys. Chem.*, 1970, **74**, 961–963.
30 J. Sandström, *Dynamic NMR Spectroscopy*, Academic Press, London, 1982.
31 M. Mauksch and P. von R. Schleyer, *Inorg. Chem.*, 2001, **40**, 1756–1769.
32 J. Cirera, E. Ruiz and S. Alvarez, *Inorg. Chem.*, 2008, **47**, 2871–2889.
33 B. Le Guennic, T. Floyd, B. R. Galan, J. Autschbach and J. B. Keister, *Inorg. Chem.*, 2009, **48**, 5504–5511.

Nickel(II)-Methyl Complexes Adopting Idealized Seesaw Geometries

Supplementary Information

Ethan A. Hill[†], Norman Zhao[†], Alexander S. Filatov, John S. Anderson*

Department of Chemistry, University of Chicago, Chicago, Illinois 60637, United States

Correspondence to: jsanderson@uchicago.edu

Table of Contents

Materials and Instrumentation

All manipulations were performed under a dry nitrogen atmosphere using either standard Schlenk techniques or in an mBraun Unilab Pro glove box unless otherwise stated. All chemicals were obtained from commercial sources and used as received unless otherwise stated. Solvents were dried on a solvent purification system from Pure Process Technologies and passed through a column of activated alumina before storing over 4 Å molecular sieves under N_2. Diethyl ether and tetrahydrofuran (THF) were stirred over NaK alloy and passed through a column of activated alumina prior to storing over 4 Å sieves under N_2. Tetraethylammonium tetrachloronickelate ($[Et_4N]_2[NiCl_4]$), $[PhB(^tBuIm)_3][OTf]_2$, 1-adamantylimidazole, and $[PhB(AdIm)_3][OTf]_2$ were prepared according to literature procedures.[1–4]

UV-vis spectra were recorded on a Thermo Scientific Evolution 300 spectrometer with the VISIONpro software suite. IR spectra were recorded on a Bruker Tensor II spectrometer with the OPUS software suite. NMR spectra for ^1H, $^{13}C\{^1H\}$, and $^{11}B\{^1H\}$ were recorded on either Bruker DRX-400 or AVANCE-500 spectrometers. ^1H and $^{13}C\{^1H\}$ spectra were referenced to residual solvent peaks. Combustion analysis was performed by Midwest Microlab. Magnetic moments were determined using the Evans method.[5]

Complex Synthesis and Characterization

*$PhB(^tBuIm)_3Ni^{II}Cl$ (**1a**):* To a Schlenk flask was added proligand $[PhB(^tBuIm)_3][OTf]_2$ (5.00 g, 6.59 mmol) and THF (100 mL). In a separate Schlenk flask, $^iPr_2NH$ (2.6 mL, 20.1 mmol) was added to THF (30 mL). Both Schlenk flasks were sealed with rubber septa, brought out of the glovebox, attached to a Schlenk line, and cooled to –78 ºC using a dry ice/isopropanol bath. A solution of ^{n}BuLi (8.1 mL, 20.1 mmol, 2.5 M in hexanes) was then added to the solution of iPr_2NH to generate lithium diisopropylamide (LDA) *in situ*. The solution of LDA in THF was then transferred via cannula to a cold suspension of the proligand. The reaction mixture was stirred at –78 ºC for approximately 45 minutes, and then solid $[Et_4N]_2[NiCl_4]$ (2.87 g, 6.92 mmol) was added under positive nitrogen pressure. After stirring at room temperature overnight, the brown reaction mixture was concentrated under vacuum to yield a green/brown residue. The flask was returned to a glovebox and triturated with hexanes (30 mL) and dried once more under vacuum. The residue was extracted into toluene (100 mL) and filtered through a pad of Celite. The resulting green solution was concentrated and redissolved in a minimal amount of toluene before layering under pentane at –35 ºC. Green crystals form after several days which are separated from a flocculent yellow/brown powder by washing with cold pentane. Crystals were dried under vacuum and lyophilized from benzene to yield pure **1a** (1.05 g, 1.90 mmol 29% yield). After separating and drying the mother liquor under vacuum, several successive crystallizations are required to achieve yields varying from 10-29%. Single crystals suitable for X-ray diffraction were grown from liquid diffusion of pentane into a concentrated solution of toluene solution of the complex at –35 ºC over several days. ^1H NMR (400 MHz, C_6D_6) δ 106.31, 15.27, 7.43, 7.26, 6.34. ^{11}B NMR (128 MHz, C_6D_6) δ −9.7. μ_{eff} (C_6D_6): 2.9 μ_B (for S = 1, μ_{SO} = 2.83 μ_B) UV-vis, nm in dichloromethane (ε, M^{-1} cm^{-1}): 446 (166), 718 (228). IR (KBr): 3142 (w), 3076 (w), 3051 (w), 3018 (w), 2978 (s), 2934 (m), 2876 (w), 1478 (w), 1432 (w), 1369 (m), 1333 (m), 1278 (s), 1232 (w), 1207 (s), 1193 (s), 1151 (s), 1123 (m), 1027 (m), 1021 (s), 931 (w), 898 (w), 880 (s), 824 (w), 806 (w), 792 (m), 722

(s), 710 (s), 700 (m), 669 (w). Anal.; Calc. for $C_{27}H_{38}N_6BNiCl$: C 58.79, H 6.94, N 15.24.; C 59.02, H 6.80, N 14.92.

*$PhB(AdIm)_3Ni^{II}Cl$ (**1b**)*: The proligand, $[PhB(AdIm)_3][OTf]_2$, was synthesized in an analogous manner to $[PhB(^tBuIm)_3][OTf]_2$ and its spectroscopic data matched previous literature.[4] To a 250 mL Schlenk flask was added $[PhB(AdIm)_3][OTf]_2$ (4.52 g, 4.55 mmol) and THF (60 mL). In a separate 50 mL Schlenk flask was added ^{i}PrNH (1.43 g, 14.0 mmol) and THF (20 mL). Both flasks were sealed with rubber septa, removed from the glovebox, and attached to a Schlenk line before cooling to −78 °C using a dry ice/isopropanol bath. After cooling, a solution of nBuLi (5.6 mL, 2.5 M in hexanes) was added via syringe to the cold ^{i}PrNH solution to generate LDA *in situ*. After briefly stirring (~5 min) the solution of LDA was transferred via cannula to a the cooled solution of $[PhB(AdIm)_3][OTf]_2$ and the mixture stirred for 1 h at −78 °C whereupon a turbid, peach-colored solution results. Under a positive flow of N_2, the septum was quickly removed and solid $[Et_4N]_2[NiCl_4]$ (2.10 g, 4.55 mmol) was added in one portion before replacing the septum. The mixture was stirred overnight and allowed to slowly warm to room temperature. The resulting brown solution was dried under vacuum at 50 °C for 1 h before returning to a glovebox. The brown residue was triturated once with hexanes (50 mL) before drying once more under vacuum. A brown, chalky residue results which is washed with several portions of room temperature toluene (typically ~50 mL in total) until a green solid remains. The green solid is transferred to a 125 mL Erlenmeyer flask and treated with hot toluene (100 °C, ~50-100 mL in total) until a green solution separates from a gray, oily solid (sometimes pale blue due to unreacted $[Et_4N]_2[NiCl_4]$). The mixture is filtered hot through a pad of Celite before drying to a green residue under vacuum. The resulting residue is dissolved in a minimum of dichloromethane (DCM) before layering under pentanes and storing at −35 °C for several days to yield dark green crystalline blocks (833 mg, 1.06 mmol, 23% yield). After separating and drying the mother liquor under vacuum, several successive crystallizations are required to achieve yields varying from 15-23%. ^{1}H NMR (400 MHz, CD_2Cl_2) δ 103.84, 13.85, 7.55-7.52, 3.79, 1.54. ^{11}B NMR (128 MHz, C_6D_6) δ −11.3. μ_{eff} (CD_2Cl_2): 3.0 μ_B (for S = 1, μ_{SO} = 2.83 μ_B) UV-vis, nm in THF (ε, M^{-1} cm^{-1}): 360 (532) 450 (171), 720 (312) 835 (sh, 80). IR (KBr): 3153 (w), 3041 (w), 2903 (s), 2847 (s), 2667 (w), 1654 (w), 1544 (w), 1454 (m), 1404 (m), 1390 (m), 1326 (m), 1277 (m), 1239 (m), 1183 (s), 1163 (s), 1125 (m), 1103 (m), 1073 (w), 1019 (s), 880 (s), 835 (m), 790 (m), 735 (m), 713 (s), 695 (m), 645 (w), 625 (w). Anal.; Calc. for $C_{45}H_{56}N_6BNiCl$: C 68.77, H 7.18, N 10.69; C 68.92, H 7.40, N 10.20.

*$PhB(^tBuIm)_3Ni^{II}Me$ (**2a**):* A solution of methyllithium (1.6 M in diethyl ether, 250 µL, 0.40 mmol) was added to a suspension of **1** (200 mg, 0.36 mmol) in diethyl ether (10 mL) at room temperature. After stirring for 30 minutes, the dark red mixture was filtered through a pad of Celite and concentrated under reduced pressure. The residue was washed with hexanes (3 x 5 mL) and dried once more under vacuum to yield a red-orange powder (71 mg, 0.13 mmol, 37% yield). Crystals suitable for X-ray diffraction were grown in a concentrated solution of diethyl ether at –35 ºC. ^{1}H NMR (400 MHz, C_6D_6) δ 8.30 (d, Ph, 2H), 7.48 (t, Ph, 2H), 7.39 (t, Ph, 1H), 7.28 (s, Im, 3H), 6.52 (s, Im, 3H), 1.60 (s, ^{t}Bu, 27H), 1.25 (br s, Me, 3H). ^{11}B NMR (128 MHz, C_6D_6) δ 1.4. ^{13}C NMR (126 MHz, C_6D_6) δ 144.2, 135.4, 127.4, 124.9, 116.6, 55.9, 31.5. UV-vis in THF: trailing UV absorbances (see below). IR (KBr): 3139 (w), 3049 (w), 2975 (s), 2925 (m), 2873 (w), 1650 (m), 1636 (m), 1475 (w), 1433 (m), 1398 (m), 1370 (m), 1337 (m), 1267 (m), 1194 (s), 1150 (m), 1110 (m), 1109 (m), 1030 (m), 931 (w), 876 (m), 826 (s), 792 (s), 737 (s), 707 (s), 638 (w). Several attempts at obtaining suitable elemental analysis data were unsuccessful. This is attributed to either

incomplete drying or decay during shipping and handling, both as a result of the thermal instability of the complex.

*PhB(AdIm)$_3$Ni^{II}Me (**2b**)*: In a 20 mL scintillation vial, **1b** (200 mg, 0.25 mmol) was dissolved in THF (10 mL). To this solution was added MeLi (225 μL, 0.36 mmol, 1.6 M solution in diethyl ether) via microsyringe. The solution was stirred for 2 h, during which time a color change from green to red occurs. The solution was dried to a red-brown residue under vacuum and extracted into toluene (15 mL) before filtering through a pad of Celite. The resulting dark red solution was layered under hexamethyldisiloxane and stored at −35 °C to yield a dark red, microcrystalline solid (99 mg, 0.13 mmol, 51% yield). Single crystals suitable for XRD were grown from toluene layered under pentane at −35 °C. ^{1}H NMR (400 MHz, C_6D_6) δ 8.34 (d, Ph, 2H), 7.50 (t, Ph, 2H), 7.41 (m, Ph, 1H), 7.30 (d, Im, 3H), 6.58 (s, Im, 3H), 2.42 (s, Ad, 18H), 2.09 (s, Ad, 9H), 1.65 (m, Ad, 18H), 1.05 (br s, Me, 3H). ^{11}B NMR (128 MHz, C_6D_6) δ 1.2. ^{13}C NMR (126 MHz, C_6D_6) δ 135.4, 128.2, 127.4, 124.4, 115.2, 56.2, 44.4, 36.7, 30.5. UV-vis in THF: broad shoulders and trailing UV absorbances (see below). IR (KBr): 3136 (w), 3060 (w), 2908 (s), 2852 (s), 2680 (w), 1644 (s), 1478 (w), 1451 (m), 1431 (w), 1398 (m), 1376 (w), 1357 (w), 1331 (m), 1307 (m), 1283 (m), 1240 (m), 1186 (m), 1169 (m), 1129 (w), 1104 (w), 1052 (w), 1026 (w), 876 (m), 835 (s), 792 (s), 736 (m), 703 (m), 680 (m). Several attempts at obtaining suitable elemental analysis data were unsuccessful. This is attributed to either incomplete drying or decay during shipping and handling, both as a result of the thermal instability of the complex.

Experimental Procedures

Crystallographic Details: The diffraction data for **2b** were measured at 110 K on a Bruker D8 fixed-chi with PILATUS1M (CdTe) pixel array detector (synchrotron radiation, λ = 0.41328 Å (30 KeV)) at the Chem-MatCARS 15-ID-B beamline at the Advanced Photon Source (Argonne National Laboratory). The diffraction data for **1a,1b,** and **2a** were measured at 100 K on a Bruker D8 VENTURE diffractometer equipped with a microfocus Mo-target X-ray tube (λ = 0.71073 Å) and PHOTON 100 CMOS detector. Data reduction and integration were performed with the Bruker APEX3 software package (Bruker AXS, version 2017.3-0, 2018). Data were scaled and corrected for absorption effects using the multi-scan procedure as implemented in SADABS (Bruker AXS, version 2014/5).[6] The structures were solved by SHELXT (Version 2014/5) and refined by a full-matrix least-squares procedure using OLEX2 (XL refinement program version 2018/1).[7–9]

Computational Methods: Geometry optimizations were performed using the ORCA program suite.[10] The O3LYP hybrid functional was used for all calculations. The basis sets for each atom were as follows: def2-TZVPP for Ni, N, and carbene C; def2-SVP for N, B, H, and remaining C.[11–13] A full frequency calculation was performed on the optimized seesaw geometry of **2a** to ensure that there were no imaginary frequencies and ensure true minima in the energies. This geometry was then optimized as a triplet to obtain the linearized geometry, which was used to generate the molecular orbitals (Figure 2 and S16) and geometry scan for the lever mechanism (Figure S17). The initial geometries were generated using crystallographic data. The geometry plots were created from the optimized xyz cartesian coordinates in Diamond 3.2.[14] The free energies of the respective species are shown in Table S3. The Kohn-Sham molecular orbitals were plotted in Avogadro with ISO values for the surface set at 0.09.[15]

Calculation of $\Delta G^{\ddagger}$ from variable temperature ^1H NMR spectroscopy: A method for determining activation barriers to exchange processes between two inequivalent species has previously been described.[16] Using this method, two different activation barriers are calculated for the two inequivalent species in solution. In this case these two species are in fact topomers, distinguished only by arbitrarily assigning the three imidazole groups and changing the orientation of the methyl ligand from between one pair to a neighboring pair. For simplicity, only one set of the coalescence temperatures and $\Delta G^{\ddagger}$ values were reported in the text where the $\Delta G^{\ddagger}$ value was calculated as the average of the A and B components with the standard deviation used as an estimate of the error. Below are the data for a total of three different resonances of each species reported here for completeness. The equation shown was used to calculate the $\Delta G^{\ddagger}$ values where Tc = coalescence temperature, X and ΔP (0.67) are related to the difference in population of the doublet,[17] and $\Delta\nu$ = difference in Hz of the fully resolved doublet of the exchanging species.

$$\Delta G^{\ddagger} = 4.575 * 10^{-3} * Tc * \left(10.62 + \log\left(\frac{X}{2\pi(1 \pm \Delta P)}\right) + \log\left(\frac{Tc}{\Delta\nu}\right)\right) \qquad (1)$$

2a	**Im (high ppm)**		**Im (low ppm)**		**^{t}Bu**	
	A	B	A	B	A	B
ν (ppm)	7.05	7.42	5.82	6.07	1.83	1.43
ν (Hz)	3526	3711	2908	3037	916	716
$\Delta\nu$ (Hz)	186		130		201	
Tc (K)	212		215		219	
$\Delta G^{\ddagger}_A$ (kcal/mol)	9.8		10.1		10.1	
$\Delta G^{\ddagger}_B$ (kcal/mol)	10.5		10.8		10.8	
Average	10.1		10.4		10.4	
Std Dev	0.5		0.5		0.5	

2b	**Im (high ppm)**		**Im (low ppm)**		**Ad**	
	A	B	A	B	A	B
ppm	7.20	7.38	5.98	6.20	2.64	2.19
Hz	3598	3690	2991	3099	1318	1094
ΔHz	92		108		224	
Tc (K)	219		225		231	
$\Delta G^{\ddagger}_A$ (kcal/mol)	10.4		10.6		10.6	
$\Delta G^{\ddagger}_B$ (kcal/mol)	11.1		11.4		11.3	
Average	10.7		11.0		11.0	
Std Dev	0.5		0.5		0.5	

Table S1: Values extracted from the variable temperature ^{1}H NMR spectra used for calculating the $\Delta G^{\ddagger}$ values for complexes **2a** and **2b**.

Figures and Tables

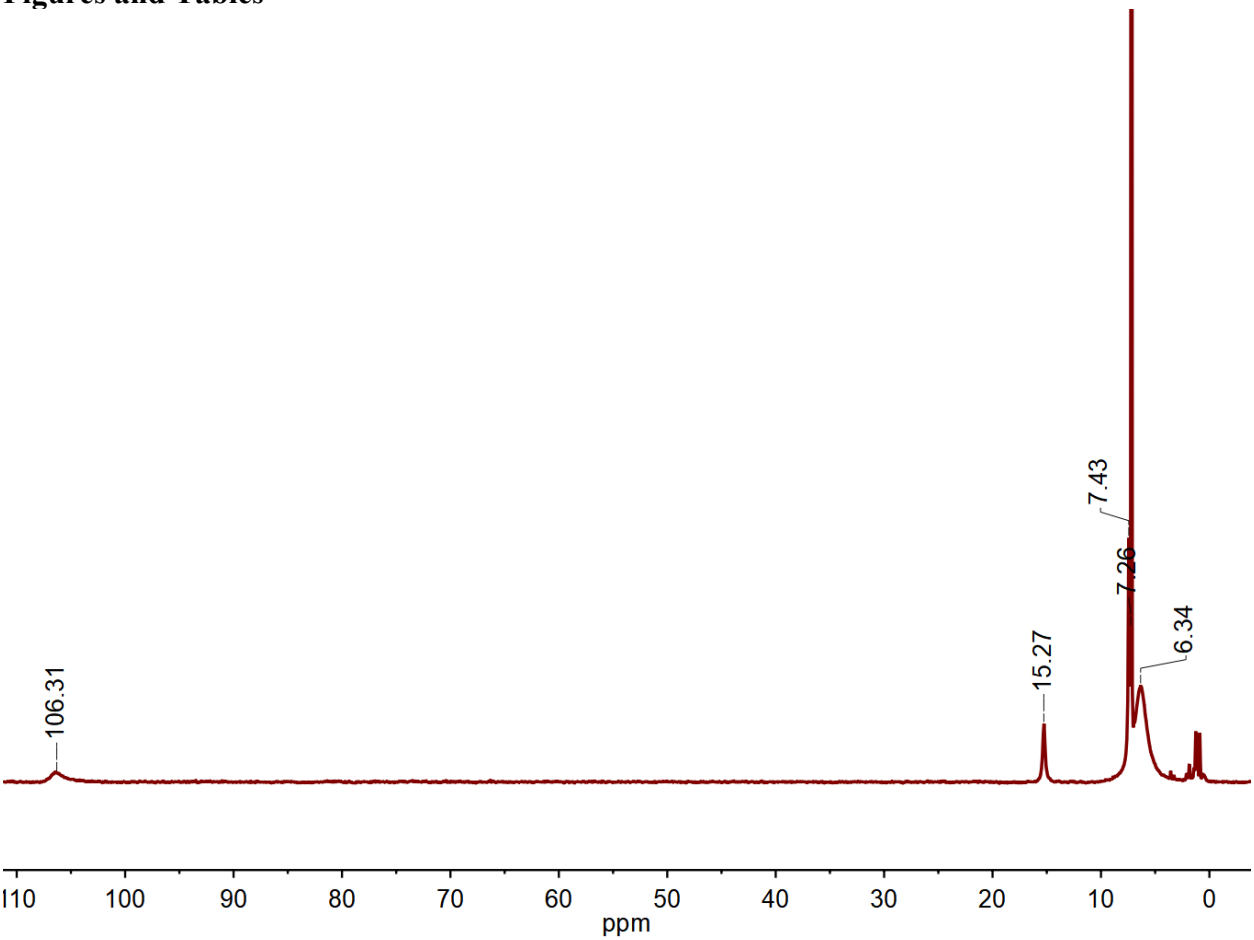

Figure S1. The paramagnetic ^{1}H NMR spectrum of **1a** in C_6D_6 at 298 K. Top of the solvent residual peak has been clipped to more clearly see paramagnetic features.

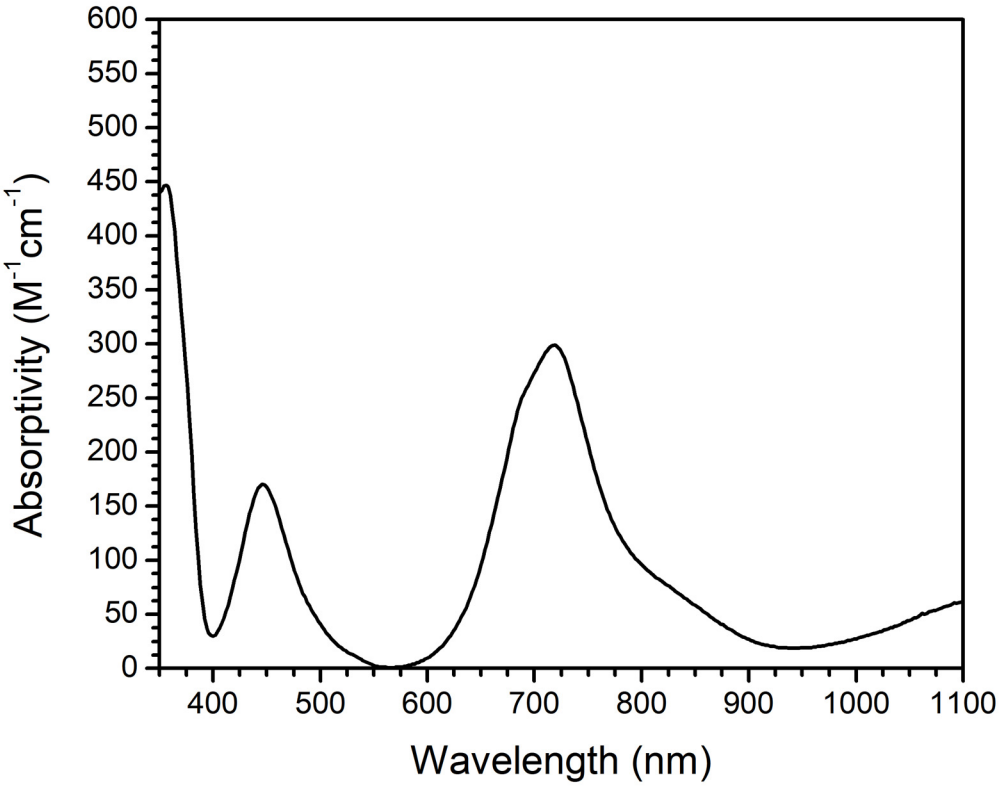

Figure S2. UV-vis spectrum of **1a** in DCM at 298 K.

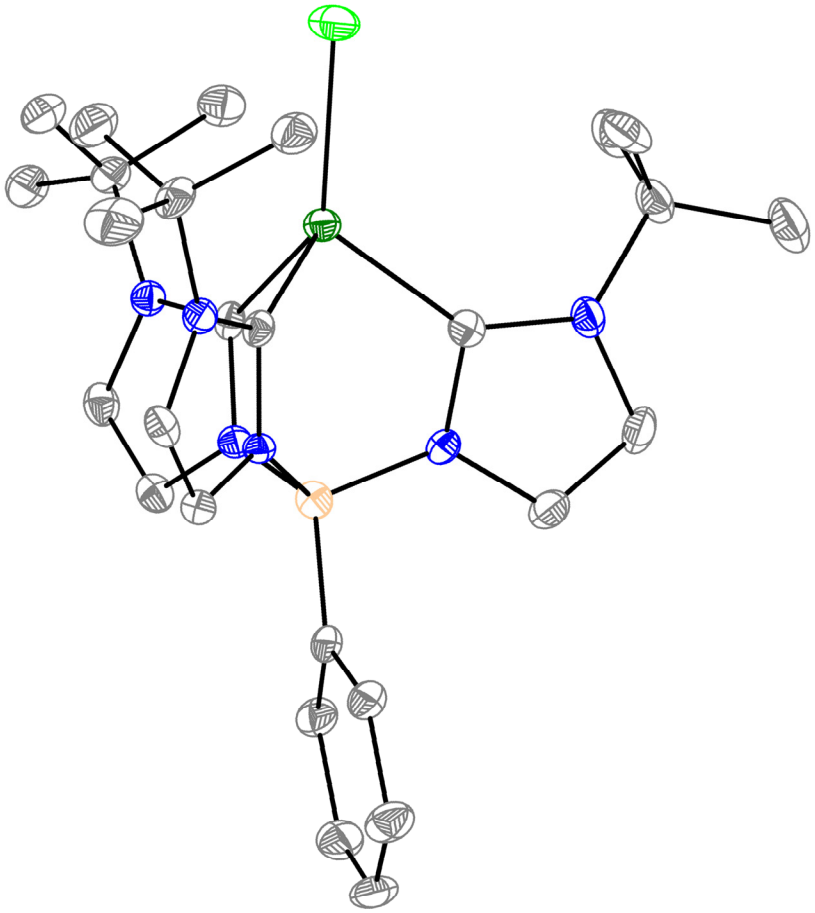

Figure S3. Molecular structure of **1a** determined by single crystal XRD. Ellipsoids drawn at 50% probability, H-atoms and solvent molecules omitted for clarity. Only one molecule in the unit cell is shown. Atom colors are dark green = Ni, light green = Cl, blue = N, tan = B, and gray = C.

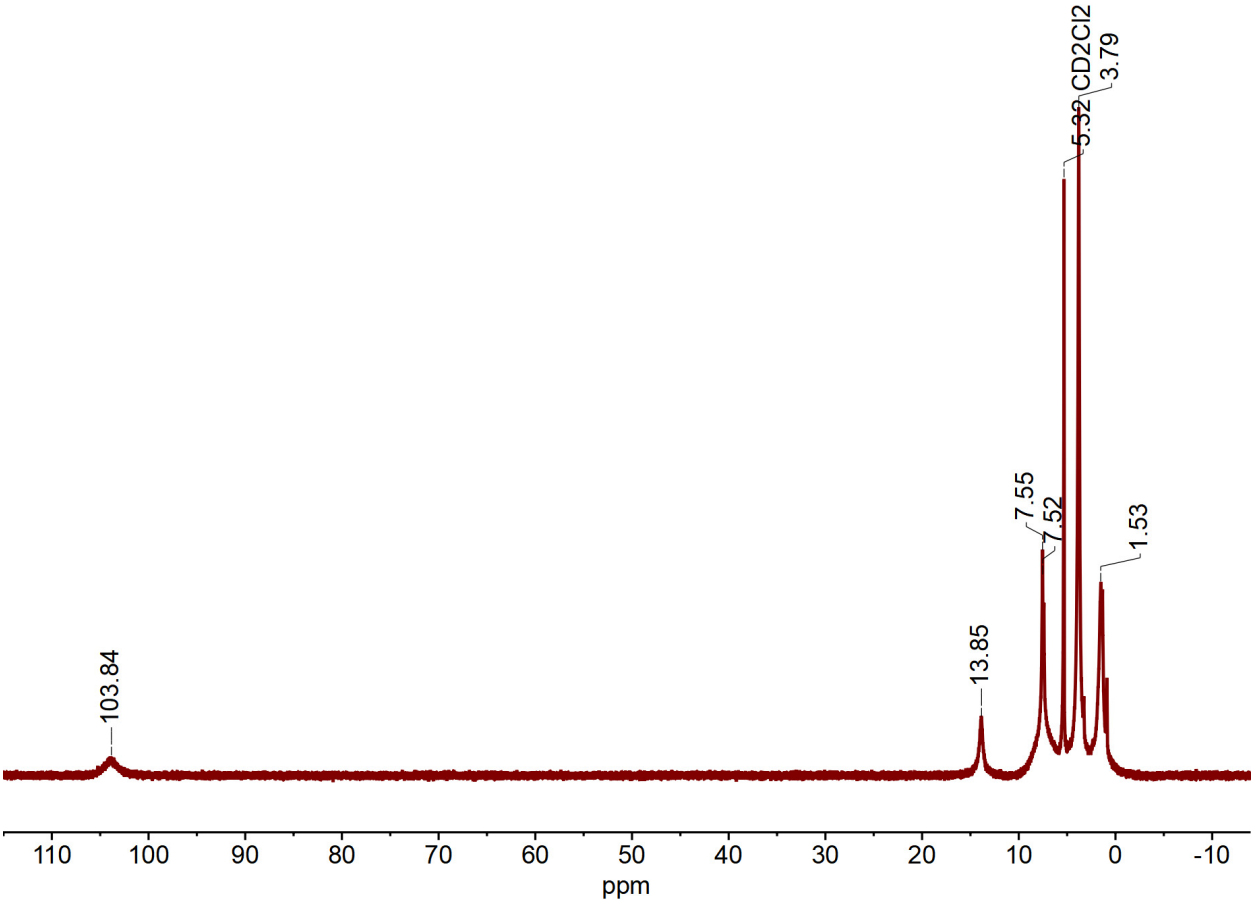

Figure S4. The paramagnetic ^{1}H NMR spectrum of **1b** in CD_2Cl_2 at 298 K.

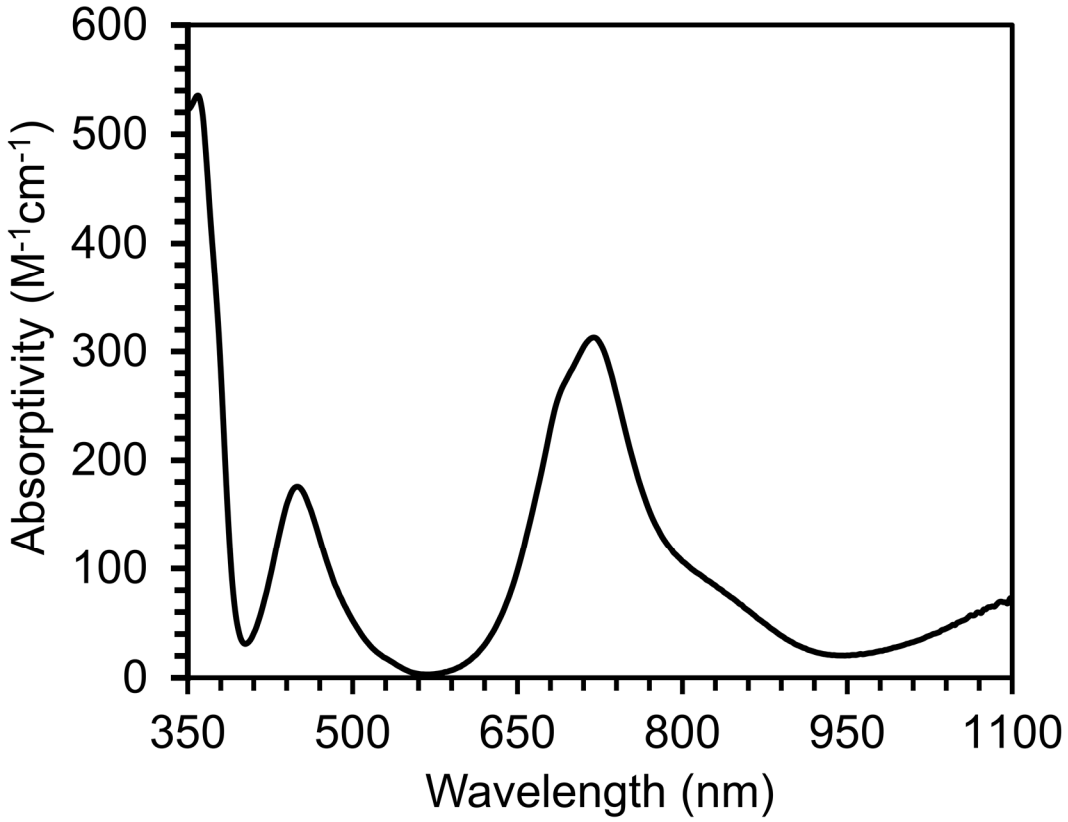

Figure S5. The UV-vis spectrum of **1b** in THF at 298 K.

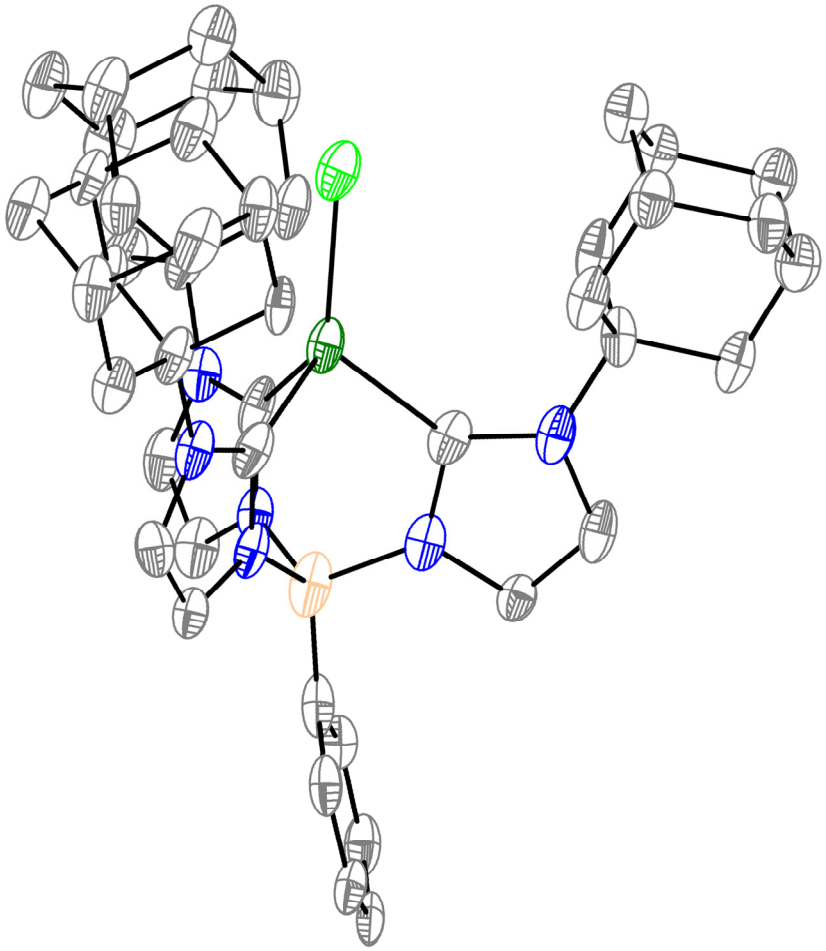

Figure S6. The molecular structure of **1b** determined by single crystal XRD. Ellipsoids drawn at 50% probability, H-atoms and solvent molecules omitted for clarity. Atom colors are dark green = Ni, light green = Cl, blue = N, tan = B, and gray = C.

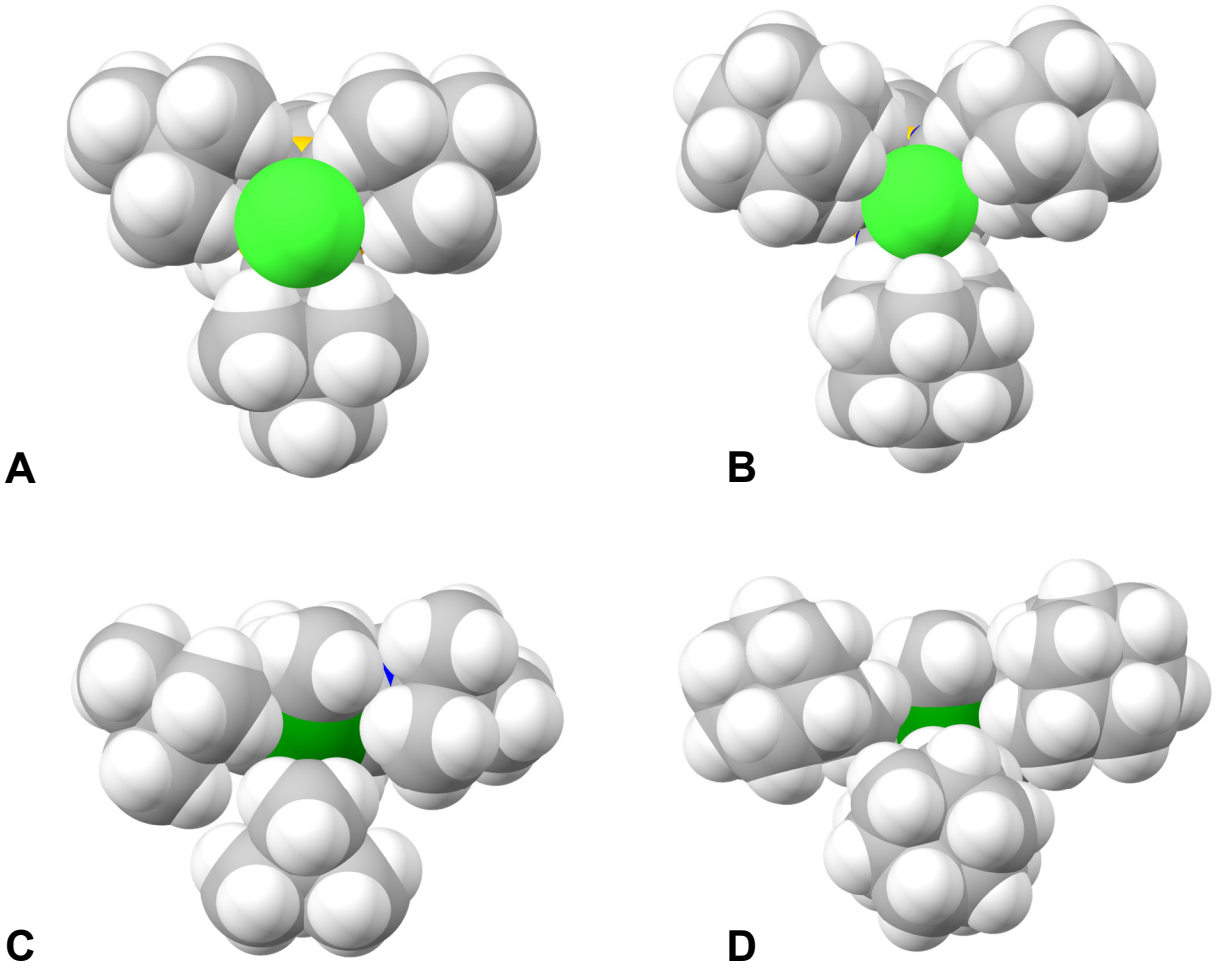

Figure S7. Depiction of the space-filling models of **1a** (A), **1b** (B), **2a** (C), and **2b** (D) to show the distortion around the nickel center due to the change in geometry. Color code: dark green = Ni, light green = Cl, gray = C, white = H, blue = N, tan = B

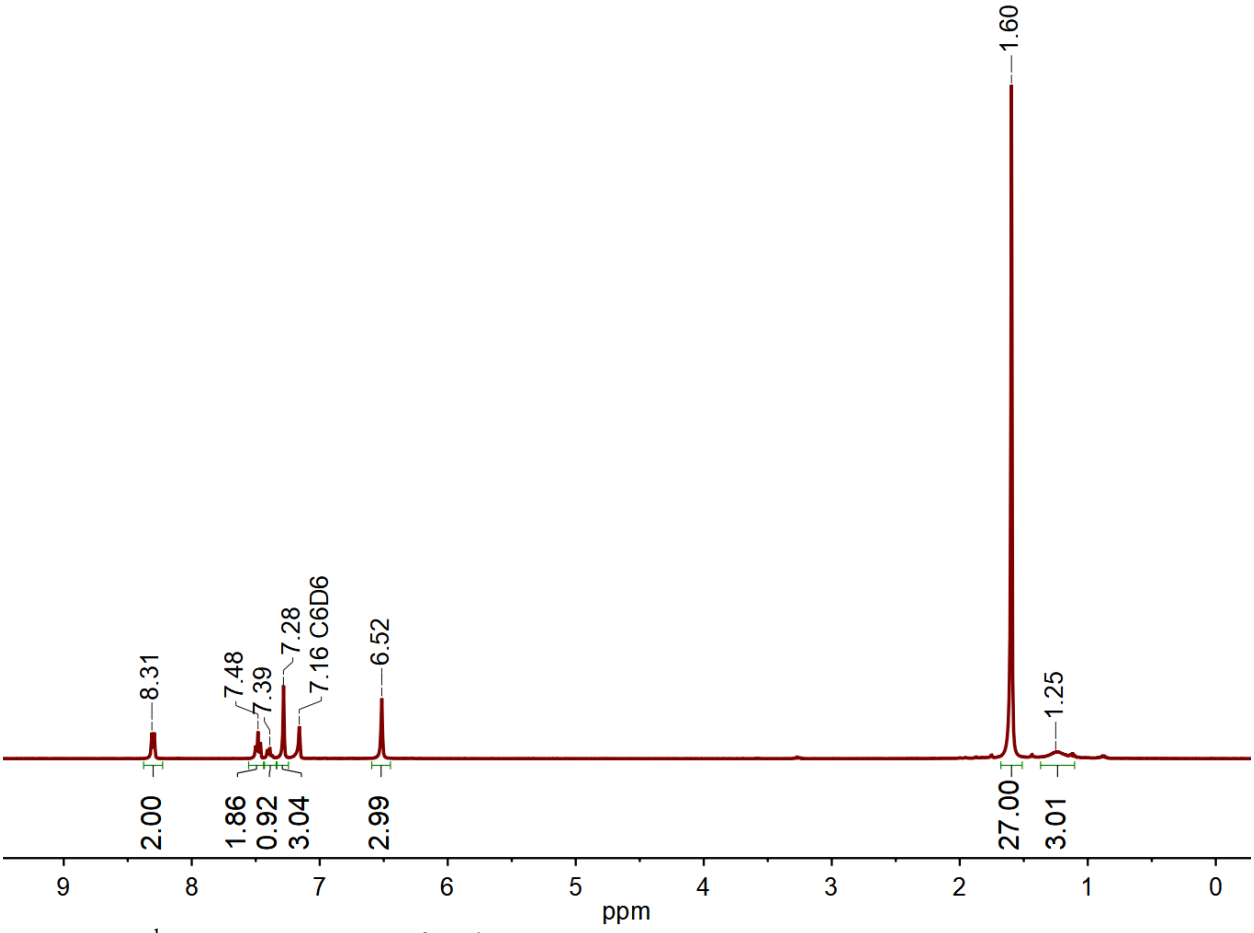

Figure S8. ^{1}H NMR spectrum of **2a** in C_6D_6 at 298 K.

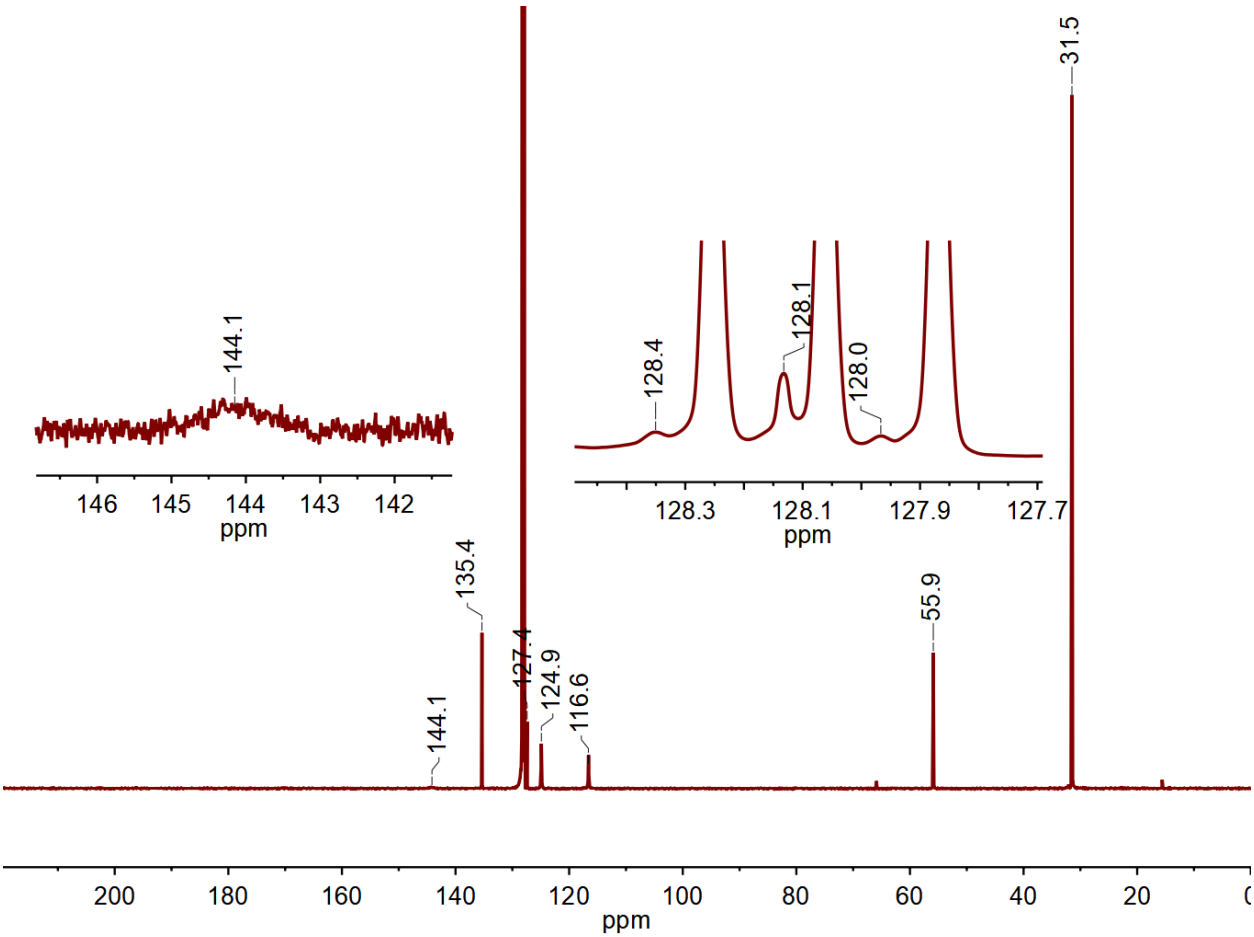

Figure S9. ^{13}C NMR spectrum of **2a** in C_6D_6 at 298 K.

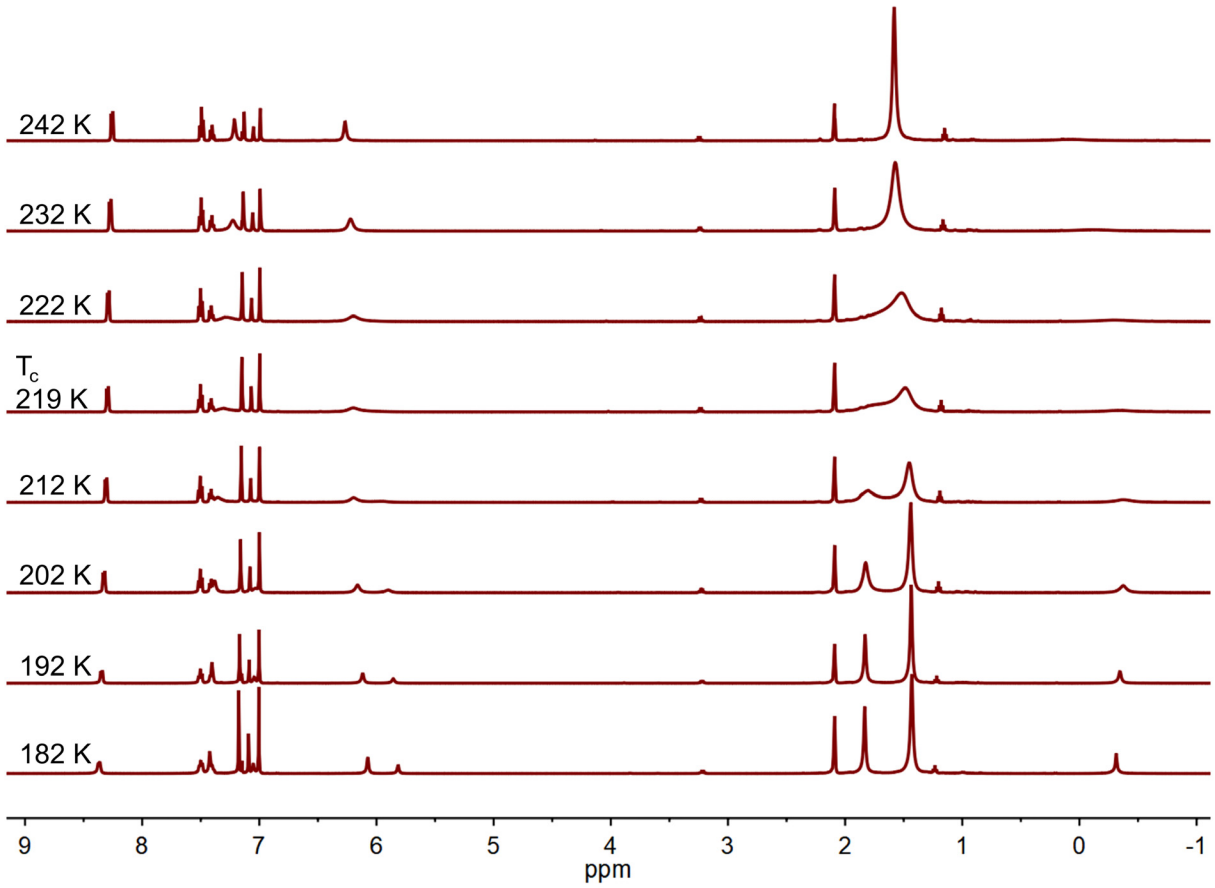

Figure S10. Variable temperature ^{1}H NMR spectra of **2a** in *d*$_8$-toluene. Reproduced here from the main text.

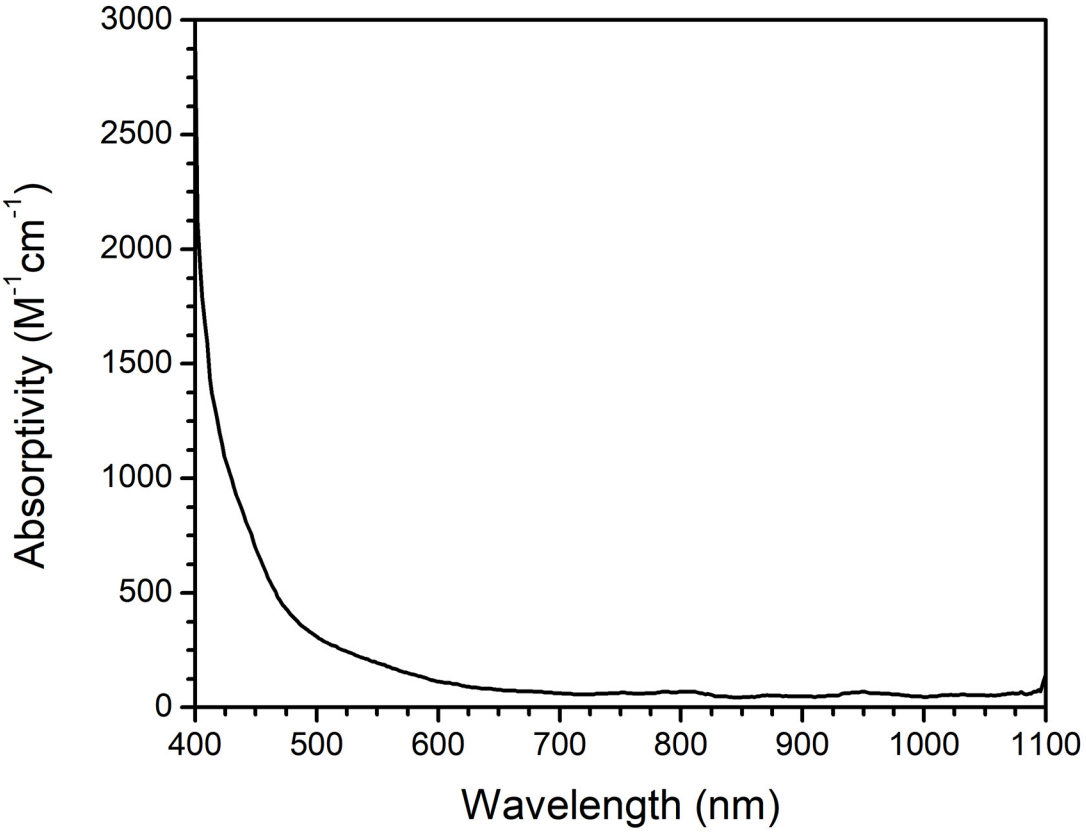

Figure S11. The UV-vis spectrum of **2a** in THF at 298 K.

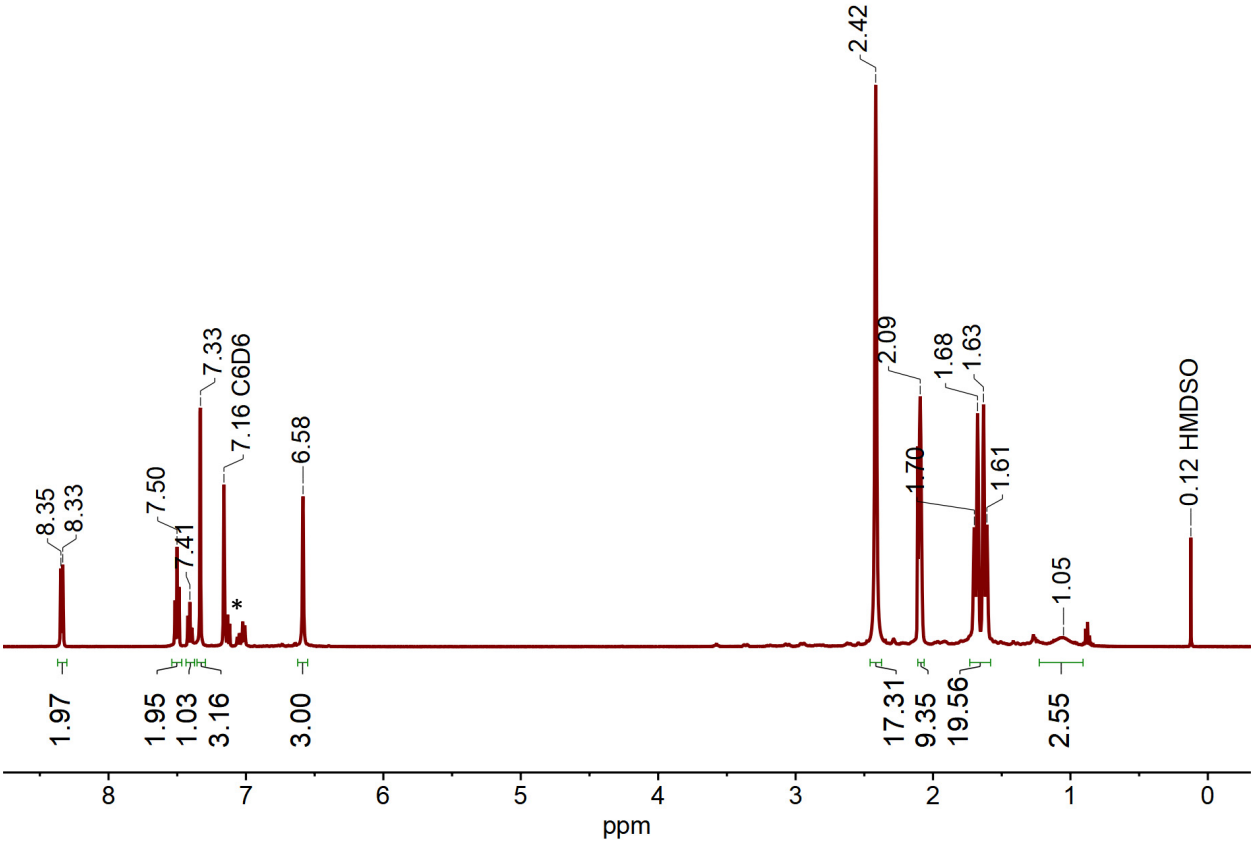

Figure S12. The ^{1}H NMR spectrum of **2b** in C_6D_6 at 298 K. Resonances for residual toluene are marked with an asterisk.

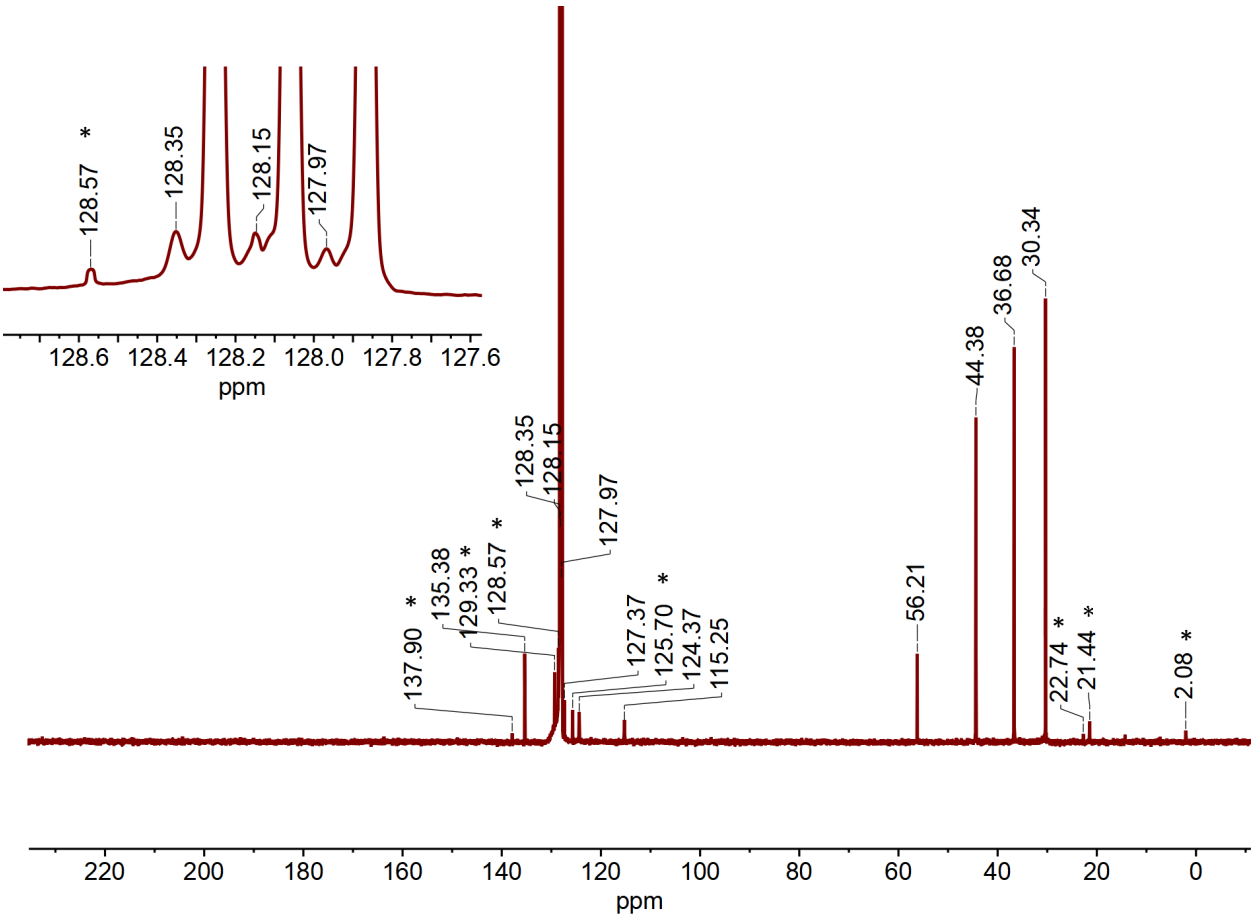

Figure S13. The ^{13}C NMR spectrum of **2b** in C_6D_6 at 298 K. Residual solvent peaks for toluene, pentane, and HMDSO marked with asterisks.

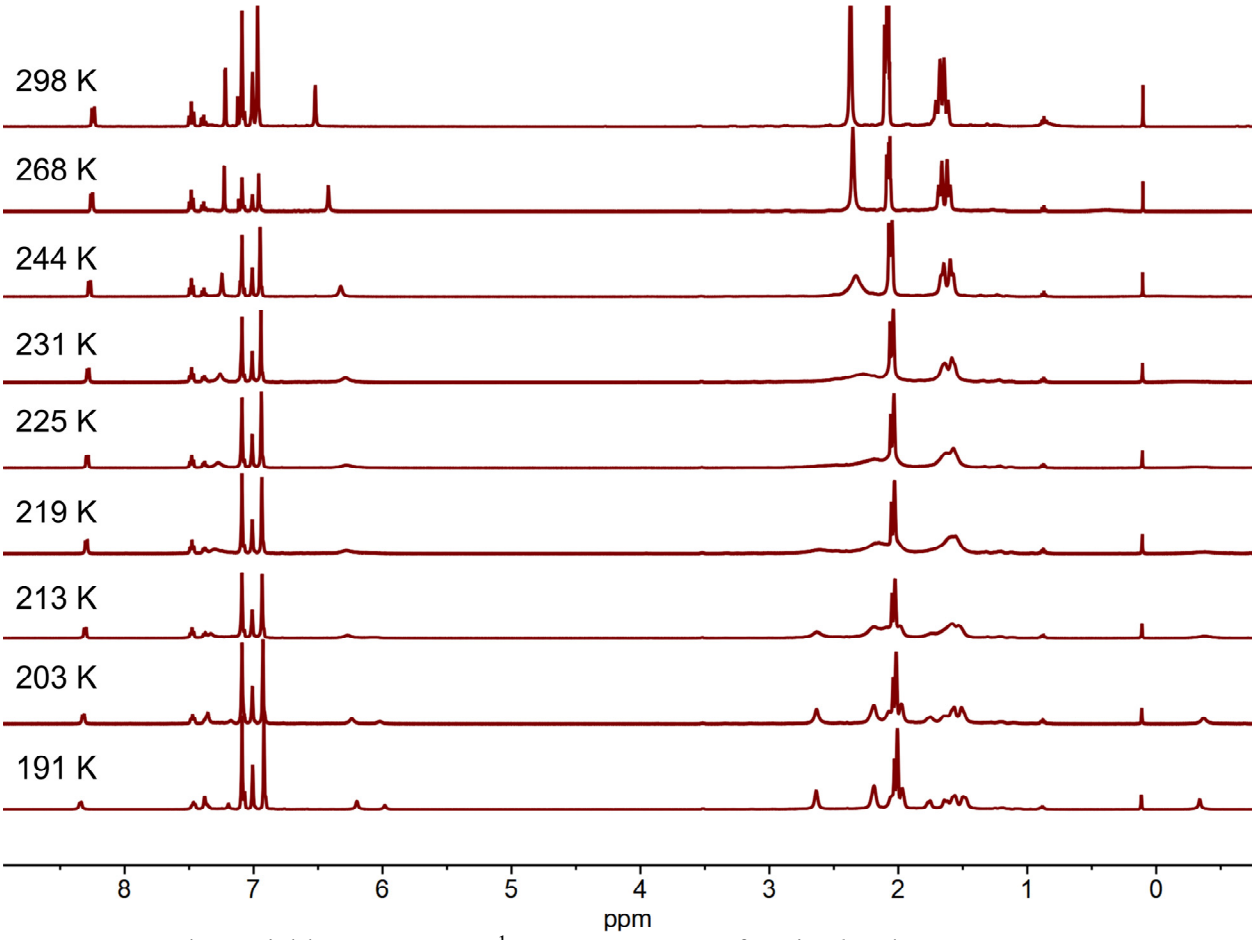

Figure S14. The variable temperature ^{1}H NMR spectra of **2b** in *d*$_{8}$-toluene.

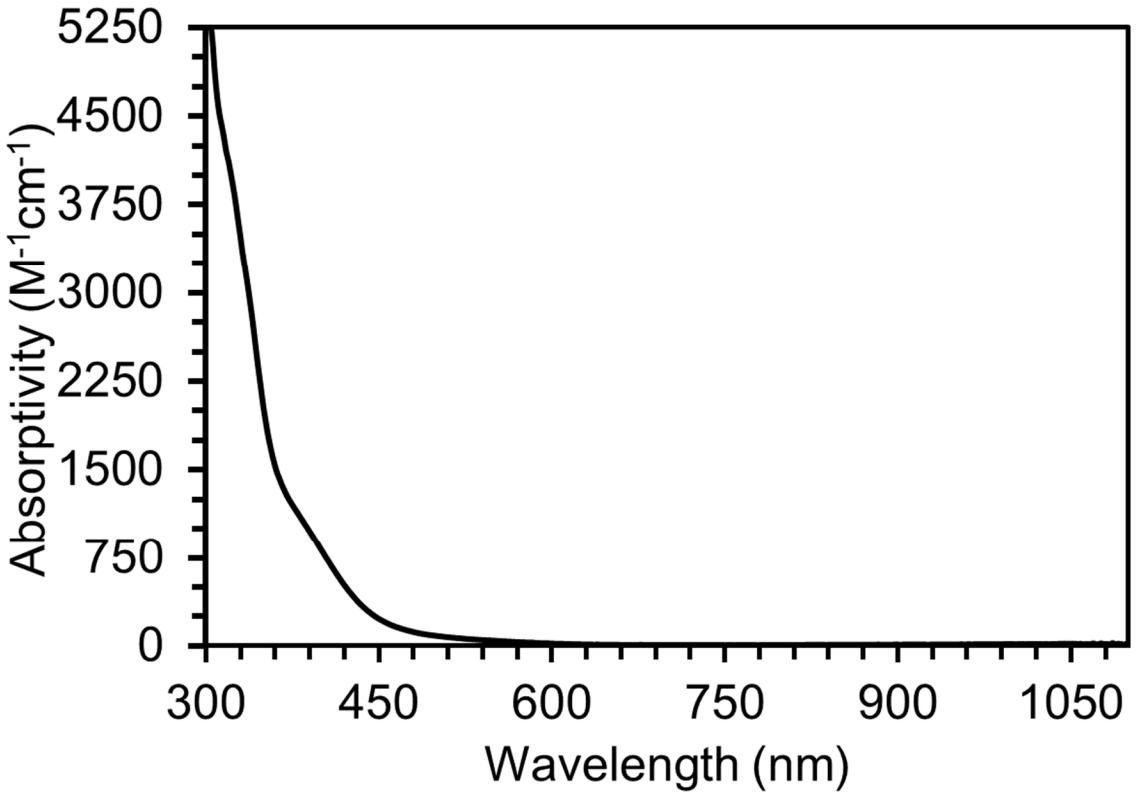

Figure S15. The UV-vis spectrum of **2b** in THF at 298 K.

Conformation	Free Energy (Hartrees)	Free Energy Difference Relative to Optimized Singlet (Hartrees)	Free Energy Difference Relative to Optimized Singlet (kcal/mol)
Optimized Singlet	-2949.7190	0	0
Triplet	-2949.7015	+0.0175	+11
Singlet, linearized	-2949.6699	+0.0491	+31

Table S2. Computed free energies of different conformations of **2a**. Note that "linearized" indicates the energy of a geometry optimization with a constrained B-Ni-C(Me) angle of 168°.

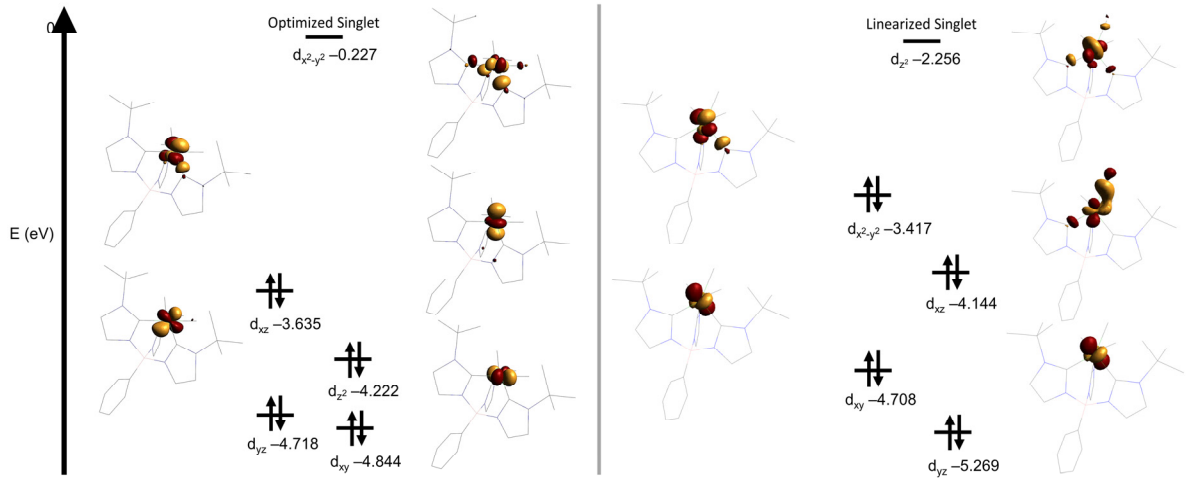

Figure S16. Kohn-Sham orbitals of **2a** in both seesaw (optimized singlet) and tetrahedral (linearized singlet) geometries in a singlet electronic configuration. Energies are qualitative.

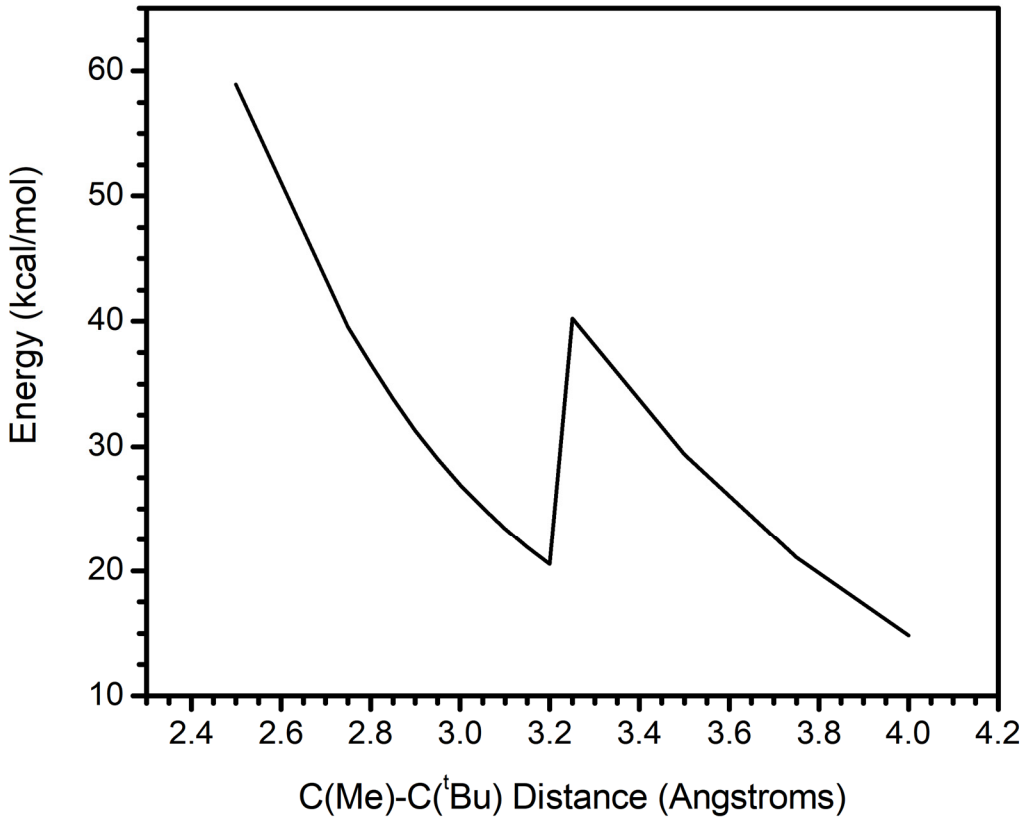

Figure S17. Plot of free energy, scanning C(Me)-C(ᵗBu) (trans) (atoms 18 and 23) distance for **2a**. Constrained dihedral angle of atoms 18, 17, 9, 23 to 0º. Energies are relative to optimized singlet (BP86). These data were used to assess the viability of a lever mechanism in the isomerization of **2a**.

2a, singlet

C	-1.883838	1.483102	-0.573295
N	-3.099486	1.859184	-1.042080
C	-3.978341	0.795105	-0.986952
C	-3.276063	-0.266658	-0.524235
N	-1.985106	0.147737	-0.322303
B	-0.744238	-0.704329	0.137471
N	0.444058	-0.217391	-0.732256
C	0.741458	1.087561	-0.688331
N	1.776530	1.270727	-1.538955
C	2.110182	0.061983	-2.128644
C	1.269498	-0.868909	-1.612267
N	-0.397591	-0.292170	1.614323
C	0.136170	0.924645	1.915647
N	0.363659	0.897403	3.252935
C	-0.112670	-0.281065	3.793790
C	-0.595655	-1.013708	2.762382
Ni	-0.394425	2.061303	0.464978
C	-1.561585	3.090002	1.633244
C	-3.476526	3.154730	-1.644169
C	-4.078316	2.883482	-3.025224
C	-4.508890	3.844065	-0.754653
C	-2.250518	4.033389	-1.823504
C	2.383794	2.562421	-1.898200
C	3.896938	2.395862	-2.004879
C	1.809399	3.015660	-3.240041
C	2.065935	3.584809	-0.818812
C	1.074473	1.902232	4.068988
C	1.771690	2.908202	3.168636
C	0.079348	2.599675	4.993796
C	2.138191	1.183919	4.900611
H	-4.318423	3.835685	-3.518211
H	-3.367514	2.334654	-3.659014
H	-5.399834	3.215693	-0.616368
H	-4.835101	4.788816	-1.212488
H	-4.091031	4.063216	0.235947
H	-1.516905	3.553200	-2.483733
H	-1.757033	4.243045	-0.869266
H	-2.558351	4.984330	-2.279783
H	4.187469	1.720502	-2.820982
H	4.318284	2.003088	-1.068551
H	4.362753	3.369388	-2.211655
H	1.999810	2.268536	-4.023484
H	2.267790	3.963988	-3.555619
H	2.514360	3.301231	0.141300
H	2.462773	4.565838	-1.114817

H	0.979294	3.677622	-0.662684
H	2.287962	3.649408	3.794645
H	2.515197	2.408989	2.533393
H	0.604161	3.319934	5.638377
H	-0.684283	3.137480	4.417844
H	2.815166	0.606004	4.255257
H	1.704142	0.497811	5.641075
H	2.737160	1.921630	5.454150
H	-5.007925	2.300636	-2.972263
H	-0.433528	1.877994	5.646189
H	0.723882	3.164105	-3.165327
C	-0.894460	-2.297069	-0.111304
C	-1.619896	-2.805435	-1.201314
C	-1.622374	-4.159179	-1.529293
C	-0.872838	-5.059957	-0.780425
C	-0.113941	-4.585206	0.284321
C	-0.124089	-3.229000	0.602676
H	-2.185673	-2.122375	-1.837569
H	-2.203575	-4.510260	-2.386271
H	-0.865438	-6.122272	-1.038275
H	0.501214	-5.274243	0.868791
H	0.512677	-2.888368	1.421752
H	-5.015927	0.865660	-1.290056
H	-3.609622	-1.277236	-0.318491
H	2.912714	-0.044054	-2.848709
H	1.202963	-1.934435	-1.804094
H	-0.064650	-0.513749	4.851009
H	-1.063586	-1.990847	2.769897
H	1.065815	3.427991	2.512419
H	-2.125824	3.855369	1.077751
H	-0.971119	3.625673	2.393411
H	-2.298581	2.472445	2.172222

2a, triplet/linearized singlet

C	-1.88569125509767	1.31575868894759	-0.43811326639217
N	-3.14878526283170	1.66052672609044	-0.80987185296364
C	-3.94040765439654	0.53817616676059	-0.90108192697676
C	-3.14599597204657	-0.52152364579506	-0.62029061451495
N	-1.88909802312851	-0.03379058089814	-0.38456748910611
B	-0.60903224830606	-0.83198993133565	0.00557003480596
N	0.58099083140707	-0.27149129747920	-0.83271162909682
C	0.90777380943085	1.02938935933492	-0.80707721709777
N	1.97312834179302	1.16251631126617	-1.63245098889613
C	2.29995694821602	-0.06055953010583	-2.18088866318950
C	1.42032371699895	-0.95844456947050	-1.67205745532825
N	-0.36843586450341	-0.43236947354582	1.49244461943455

C	-0.10533824350746	0.84820227285494	1.82843366705584
N	0.02261740134565	0.84291570040751	3.18321152202865
C	-0.22023097826837	-0.41772507595790	3.67889590463566
C	-0.47793161906641	-1.21136645578209	2.61185751330369
Ni	-0.21634134244536	2.22182346247562	0.32048308862942
C	-0.34394784346457	4.21078585103639	0.79704147734641
C	-3.64591573532743	3.02874174745787	-1.08787655384876
C	-4.92339356174412	2.95173733071580	-1.91932830642893
C	-3.94045382901606	3.72405757207476	0.23584824375981
C	-2.59307235294179	3.77512114962372	-1.89407119550272
C	2.62977777703495	2.44826959973971	-1.95403282701069
C	3.90073640965399	2.19241724973042	-2.75375811856548
C	1.66161813088817	3.28486156941171	-2.78499761553622
C	2.98739265833306	3.16605494334824	-0.65881066072034
C	0.37277851918442	2.01030408111675	4.02513000073215
C	1.64510549502002	2.63707289344975	3.46735633764218
C	-0.80009949187798	2.98239307544404	4.00780168947619
C	0.64266889101337	1.56696546395433	5.45921957389298
H	-5.21600297179344	3.96966258314931	-2.20905498004265
H	-4.77483538139672	2.37195058839875	-2.84158518608729
H	-4.70192302408444	3.16848926704650	0.80170413322900
H	-4.31989971031230	4.74136685954890	0.05973376999149
H	-3.03009909980279	3.79110938650242	0.84167894429443
H	-2.39043153345005	3.25570153156292	-2.84135666891313
H	-1.65812106645400	3.85424467407422	-1.33011623309714
H	-2.94852498820488	4.78893968169072	-2.12469646380177
H	3.69399680593918	1.72896672075373	-3.72866535039449
H	4.60789604917539	1.55695288865215	-2.20166369695313
H	4.39734267406814	3.15177645780343	-2.94973295493965
H	1.37208364888784	2.75054014002131	-3.70124456961360
H	2.12549371185625	4.23873036015142	-3.07341042036880
H	3.65586715875062	2.55080448900828	-0.04059036220796
H	3.49651519664244	4.11397553924886	-0.88305329914110
H	2.08613294515885	3.39678713747206	-0.07657822616097
H	1.92373382864089	3.52210600736703	4.05647836656728
H	2.47543650299482	1.91723804804511	3.50657943155703
H	-0.57145944934482	3.87307972585939	4.60968611547596
H	-1.01744314229579	3.30097893440695	2.98203306983669
H	1.44835055936570	0.82085714842141	5.51828563746324
H	-0.25224679482502	1.16171583159217	5.95138627702716
H	0.96219464561195	2.44370658387497	6.03892175630851
H	-5.76737807001261	2.52157277057606	-1.36262943550942
H	-1.69705648114461	2.50471205252176	4.42856482067915
H	0.75106168820002	3.50533312663273	-2.21252783332477
C	-0.67848552588422	-2.42277801842856	-0.29411299961316
C	-1.37397106180094	-2.93281761939183	-1.40312066318050

C	-1.31706870733429	-4.27597537566095	-1.76725055563931
C	-0.53413177577185	-5.16437885729610	-1.03811679492938
C	0.20005203023307	-4.68574699426628	0.04171834071536
C	0.13006038421287	-3.34031831262337	0.39598458795563
H	-1.96020529396477	-2.25878358409135	-2.03025686539491
H	-1.87735065767084	-4.62705649924771	-2.63788073762899
H	-0.47928159742132	-6.21779254316468	-1.32438380876072
H	0.84382746208976	-5.36241272051518	0.60948660431295
H	0.75611429242425	-2.99582335963794	1.22126897797971
H	-4.98834102951826	0.56457244584578	-1.16633260680204
H	-3.39687016065218	-1.57356254922776	-0.56190190759963
H	3.11669580178656	-0.20972105062183	-2.87458595934619
H	1.33639413746554	-2.02451901709759	-1.84794642922798
H	-0.19535956937821	-0.66498041913484	4.73175078062579
H	-0.75011003680776	-2.25892919638108	2.58057951498498
H	1.49929255829484	2.94936774080259	2.42815866711068
H	-0.20077032183951	4.82393582181974	-0.11392781876201
H	0.46806444728223	4.52826774727787	1.47559528470696
H	-1.26779673026511	4.59857317178742	1.25620045505045

Table S3. Optimized coordinates for DFT optimized geometries of **2a**.

Identification code	**1a**	**1b**	**2a**	**2b**
Empirical formula	$C_{27}H_{38}BClN_6Ni$	$C_{45.7}H_{57.4}BCl_{2.4}N_6Ni$	$C_{28}H_{41}BN_6Ni$	$C_{46}H_{59}BN_6Ni$
Formula weight	551.60	845.37	531.19	765.51
Temperature/K	100(2)	100(2)	100(2)	110(2)
Crystal system	monoclinic	monoclinic	triclinic	tetragonal
Space group	$P2_1/n$	$P2_1/n$	P-1	$I4_1/a$
a/Å	9.6383(16)	19.896(3)	9.8692(5)	34.481(3)
b/Å	17.821(3)	11.9883(15)	12.4359(7)	34.481(3)
c/Å	16.177(3)	21.333(3)	12.6239(7)	13.9826(14)
α/°	90	90	99.808(2)	90
β/°	91.925(6)	107.846(3)	97.233(2)	90
γ/°	90	90	113.118(2)	90
Volume/Å^3	2777.0(8)	4843.3(11)	1371.98(13)	16625(3)
Z	4	4	2	16
ρ_{calc}g/cm^3	1.319	1.159	1.286	1.223
μ/mm^{-1}	0.822	0.568	0.735	0.127
F(000)	1168.0	1790.0	568.0	6560.0
Crystal size/mm^3	0.48 × 0.28 × 0.19	0.35 × 0.31 × 0.21	0.298 × 0.295 × 0.153	0.03 × 0.03 × 0.03
Radiation	MoKα (λ = 0.71073)	MoKα (λ = 0.71073)	MoKα (λ = 0.71073)	synchrotron (λ = 0.41328)
2Θ range for data collection/°	4.572 to 50.148	4.78 to 50.81	4.504 to 55.016	1.374 to 32.464
Index ranges	-11 ≤ h ≤ 11, -21 ≤ k ≤ 20, -19 ≤ l ≤ 19	-24 ≤ h ≤ 23, -14 ≤ k ≤ 14, -25 ≤ l ≤ 25	-12 ≤ h ≤ 12, -16 ≤ k ≤ 16, -16 ≤ l ≤ 16	-46 ≤ h ≤ 46, -46 ≤ k ≤ 46, -18 ≤ l ≤ 18
Reflections collected	25048	59965	37813	252183
Independent reflections	4930 [R_{int} = 0.0560, R_{sigma} = 0.0487]	8900 [R_{int} = 0.0944, R_{sigma} = 0.0736]	6259 [R_{int} = 0.0424, R_{sigma} = 0.0366]	10760 [R_{int} = 0.0435, R_{sigma} = 0.0120]
Data/restraints/parameters	4930/0/334	8900/0/514	6259/0/335	10760/0/488
Goodness-of-fit on F^2	1.014	1.032	1.055	1.087
Final R indexes [I>=2σ (I)]	R_1 = 0.0385, wR_2 = 0.0847	R_1 = 0.1004, wR_2 = 0.2515	R_1 = 0.0345, wR_2 = 0.0691	R_1 = 0.0412, wR_2 = 0.0984
Final R indexes [all data]	R_1 = 0.0633, wR_2 = 0.0939	R_1 = 0.1419, wR_2 = 0.2746	R_1 = 0.0484, wR_2 = 0.0737	R_1 = 0.0434, wR_2 = 0.0997
Largest diff. peak/hole / e Å^{-3}	0.56/-0.23	1.31/-1.15	0.56/-0.33	0.49/-0.43

Table S4. Crystal structure refinement details for complexes **1a**, **1b**, **2a**, and **2b**.

References

1 N. S. Gill and R. S. Nyholm, *J. Chem. Soc.*, 1959, **0**, 3997.

2 R. E. Cowley, R. P. Bontchev, E. N. Duesler and J. M. Smith, *Inorg. Chem.*, 2006, **45**, 9771–9779.

3 Y. Xiong, S. Yao, T. Szilvási, E. Ballestero-Martínez, H. Grützmacher and M. Driess, *Angew. Chem., Int. Ed.*, 2017, **56**, 4333–4336.

4 Y. Fan, J. Cheng, Y. Gao, M. Shi and L. Deng, *Acta Chim. Sin.*, 2018, **76**, 445–452.

5 D. F. Evans, *J. Chem. Soc.*, 1959, 2003–2005.

6 G. M. Sheldrick, *SHELXTL*, 2014.

7 G. M. Sheldrick, *Acta Crystallogr.*, 2015, **A71**, 3–8.

8 G. M. Sheldrick, *Acta Crystallogr.*, 2015, **C71**, 3–8.

9 L. Krause, R. Herbst-Irmer, G. M. Sheldrick and D. Stalke, *J. Appl. Crystallogr.*, 2015, **48**, 3–10.

10 F. Neese, *Wiley Interdiscip. Rev. Comput. Mol. Sci.*, 2012, **2**, 73–78.

11 F. Weigend and R. Ahlrichs, *Phys. Chem. Chem. Phys.*, 2005, **7**, 3297–3305.

12 A. Schäfer, C. Huber and R. Ahlrichs, *J. Chem. Phys.*, 1994, **100**, 5829–5835.

13 A. Schäfer, H. Horn and R. Ahlrichs, *J. Chem. Phys.*, 1992, **97**, 2571–2577.

14 D. H. Putz and D. K. Brandenburg, *Diamond - Crystal and Molecular Structure Visualization, Crystal Impact*, GbR, Kreuzherrenstr. 102, 53227 Bonn, Germany.

15 M. D. Hanwell, D. E. Curtis, D. C. Lonie, T. Vandermeersch, E. Zurek and G. R. Hutchison, *J. Cheminform.*, 2012, **4**, 17.

16 H. Shanan-Atidi and K. H. Bar-Eli, *J. Phys. Chem.*, 1970, **74**, 961–963.

17 J. Sandström, *Dynamic NMR Spectroscopy*, Academic Press, London, 1982.

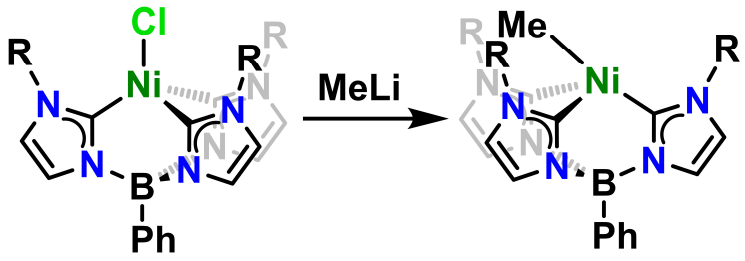

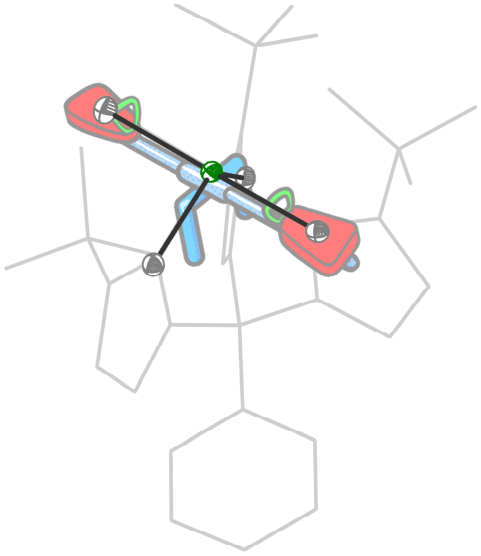

Electronically Preferred Seesaw Geometries in Ni Alkyl Complexes

Tris-carbene borate supported nickel methyl complexes adopt unusual seesaw geometries due to competing electronic and chelate effects.